Research Article

Wensheng Zhao, Guotao Fang, Xiao Qin*, and Jie Mao

Multiscale characterization of the UV aging resistance and mechanism of light stabilizer-modified asphalt

https://doi.org/10.1515/rams-2023-0152
received July 01, 2023; accepted December 06, 2023

Abstract: To clarify the effect and mechanism of hindered amine light stabilizer (HALS) on the UV aging behavior of asphalt binder, T622-HALS was selected as the modifier for UV aging resistance of asphalt. The physicochemical properties and microstructure of T622 light stabilizer were comprehensively analyzed. The light stabilizer-modified asphalt was prepared and placed in the UV radiation chamber for UV aging treatment. Scanning electron microscope and atomic force microscope were used to analyze the microscopic morphology evolution of light stabilizer-modified asphalt induced by UV radiation. The thermal properties and functional group composition changes in light stabilizer-modified asphalt during UV aging were studied by using the thermogravimetric and infrared spectroscopy combined testing system. The decay laws of the physical and rheological performances of light stabilizer-modified asphalt were studied during UV aging process, and the effect of light stabilizer on the UV aging behavior of asphalt binder was clarified. The research results indicated that HALSs could alleviate the microcracks and roughness change on the surface of asphalt and reduce the content of functional groups such as carbonyl and sulfoxide in asphalt. Furthermore, HALS could reduce the value difference of physical and rheological properties of asphalt before and after UV aging, significantly improving the UV aging resistance of asphalt binder.

Keywords: asphalt, UV aging, characterization

1 Introduction

Asphalt pavement is prone to material and structural durability issues during service, leading to service failure. The aging of asphalt due to heat and ultraviolet radiation is an important factor leading to the degradation of asphalt pavement performance, which is a particularly common problem in high-altitude areas [1,2]. Asphalt aging behavior could be mainly derived from its molecular structure changes irreversibly with UV radiation or heat effect, resulting in degraded flexibility of asphalt mixture and cracking problem [3,4]. The aging of asphalt mainly includes two types: ultraviolet aging and thermal oxygen aging, among which ultraviolet aging mainly refers to the aging of asphalt during the application of pavement in the open traffic environment. Thermal oxygen aging refers to the aging of asphalt during production, storage, transportation, as well as the mixing, transportation, and paving stages of asphalt mixtures [5]. To mitigate the UV aging problem of asphalt pavement during application, light absorbing or shielding materials could be added to the asphalt to enhance its resistance to UV aging by shielding UV light, isolating oxygen, or capturing oxygen-containing free radicals [6,7]. Currently, the main modifying agents used in asphalt consist of carbon black, nano oxides, layered silicates, UV absorbers, and layered double hydroxy composite metal hydroxides [8–12]. These commonly used modifying agents could improve the UV light aging resistance of asphalt [13]. However, the addition of carbon black and layered silicate would reduce the low-temperature performance of asphalt. The compatibility between nano oxide, layered double hydroxyl composite metal hydroxide, and asphalt is poor, which would lead to the degradation of UV resistance [14,15]. As a new type of asphalt aging control agent, ultraviolet light absorbers have good compatibility with asphalt and excellent dispersibility, gradually becoming one of the important choices for ultraviolet aging control of pavement materials.

* **Corresponding author: Xiao Qin**, School of Transportation and Civil Engineering and Architecture, Foshan University, Foshan 528000, China, e-mail: qinnao@126.com
Wensheng Zhao: National Engineering Research Center of Highway Maintenance Technology, Changsha University of Science & Technology, Changsha, 410114, China; School of Traffic & Transportation Engineering, Changsha University of Science & Technology, Changsha, 410114, China
Guotao Fang: Guangzhou HuaHui Traffic Technology Co.,Ltd., Guangzhou 510335, China
Jie Mao: Engineering Department, Guangdong GuanYue Highway & Bridge Co., Ltd., Guangzhou 511450, China

As an excellent UV absorber, hindered amine light stabilizer (HALS) could achieve UV resistance improvement through multiple ways such as decomposing hydroperoxide, quenching excited state oxygen, and capturing free radicals, of which the most typical mechanism is to capture free radicals [16]. HALS belongs to the class of free radical trapping agents in light stabilizers, which could effectively inhibit the photolysis of organic polymer compounds, have low mobility, and withstand long-term oxidation [17–19]. The HALS achieves UV aging resistance by quenching singlet oxygen, capturing free radicals, and decomposing hydrogen peroxide compounds [20]. HALSs have been gradually applied as modifiers in asphalt binders due to their excellent resistance to UV aging, thereby forming a good inhibitory effect on the UV aging behavior of asphalt binders. Regarding the main UV resistance-improving mechanism of HALS, researcher explored through different aspects. For quenching singlet oxygen, researchers [21–24] found that the conjugated structural groups contained in organic polymer materials absorb the energy of ultraviolet rays to produce singlet oxygen and R–O radicals. R–O· radicals would trigger HALS to generate hindered amine nitrogen oxygen radical compounds, which could efficiently reduce the energy of singlet oxygen in the electronic excited state and transform it into the oxygen stable state. Regarding capturing free radicals, current studies supposed that HALS is the derivative of tetramethylpiperidine, which is oxidized by peroxides generated by polymer light to form stable tetramethylpiperidine nitroxide radicals. It could efficiently capture alkyl, alkoxy, and peroxyalkyl radicals generated by UV excitation, generate stable compounds without destructive effects, and continue to interact with the radicals to regenerate tetramethylpiperidine nitroxide radicals [25,26]. For decomposing hydrogen peroxide compounds, HALS could effectively convert hydrogen peroxide compounds into highly efficient and stable nitrogen oxygen free radical compounds [27,28]. At present, research on the use of HALSs for the control of asphalt UV aging mainly focuses on the rheological properties and changes of internal microstructure or components of modified asphalt after UV aging. Feng and Xu [29,30] investigated the impact of HALS on the technical property of asphalt and revealed that HALS could achieve the UV aging delay of asphalt and also could improve the thermal stability of asphalt. Zhang [6] focused on the rheological properties of HALS-modified asphalt and proposed the optimal evaluating indices of rheological properties. Liu and Sun [13] explored the effect of HALS on the micro-structure and functional group, which confirms the improving effect of HALS of UV resistance of asphalt. Yu and Qian [19,31] clarified the variation of microstructure during the whole UV aging period and confirmed the typical UV aging microstructure of asphalt. Although the results of current studies clarify the feasibility of HALS in asphalt pavement materials, the actual improving effect of HALS is uncertain and unstable because of unclear mechanisms. Moreover, there is a lack of research on the actual intervention mechanism of HALSs on asphalt UV aging behavior [32]. However, the chemical composition of asphalt materials is extremely complex, which has significant differences from polymer materials of certain molecular chain configurations and degree of polymerization. Simply replicating the application experience of HALS in polymer materials has certain blindness for the UV aging control of asphalt pavement materials, which also makes it difficult for HALS to maintain efficient and stable performance during the UV aging resistance of asphalt binder.

Based on this research gap, for the purpose of exploring the effect and mechanism of HALS on the UV resistance of asphalt, this article selects T622 HALS as the modifier and investigates the impact of T622 on the performance, microstructure, and chemical composition to explore its effect mechanism on asphalt. Scanning electron microscope (SEM) and atomic force microscope (AFM) were used to analyze the microscopic morphology evolution of light stabilizer-modified asphalt induced by UV aging. The thermal properties and functional group composition changes in light stabilizer-modified asphalt during UV aging process were studied by applying the thermogravimetric and infrared spectroscopy combined testing system. The characteristics of rheological performance, micromorphology, and chemical property of light stabilizer-modified asphalt were systematically studied during the whole UV aging process to clarify the effect and mechanism of HALS on the UV aging behavior of asphalt binder.

2 Materials and methods

2.1 Materials

2.1.1 Light stabilizer

Based on the excellent application effect of light stabilizer in polymer, Tinuvin622 (T622) HALS was preferred as anti-aging agent to prepare modified asphalt. Its molecular formula is $C_{15}H_{29}NO_6$, molecular weight is 319.4, and fineness is 300 mesh. The application dosage of light stabilizer in asphalt was 0.2–0.8%, and the selected HALS was purchased from Guangzhou Honghai New Materials Technology Co., Ltd. The mechanism of HALSs when blended with asphalt is shown in Figure 1.

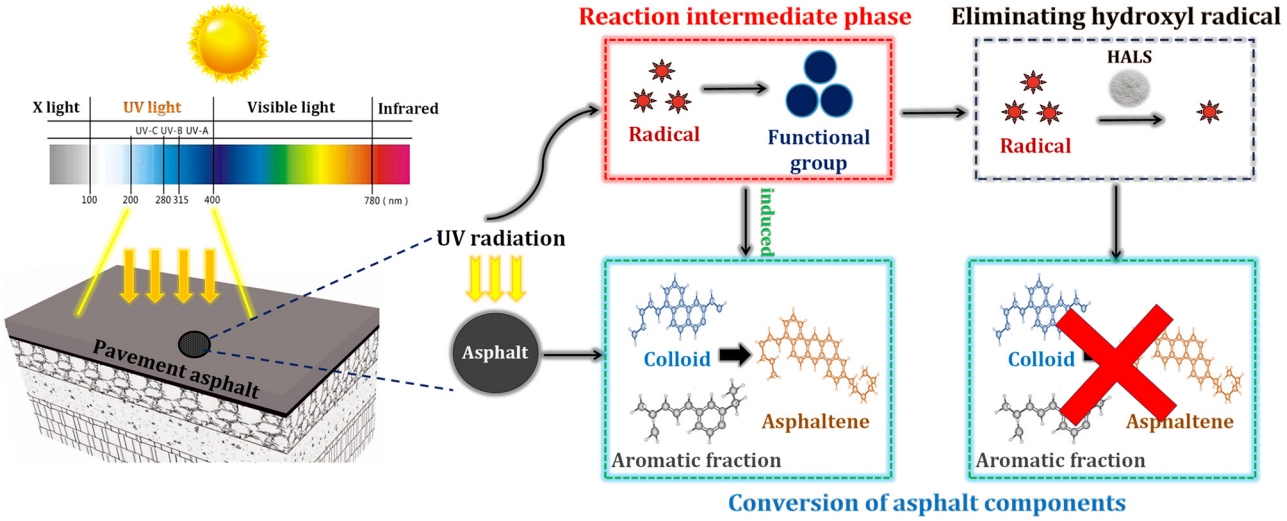

Figure 1: Mechanism of hindered amine light stabilizers when blended with asphalt.

2.1.2 Asphalt

70# base asphalt was selected as the carrier for the preparation of light stabilizer-modified asphalt. The technical performance of 70# base asphalt was tested according to the "Test Specification for Asphalt and Asphalt Mixtures in Highway Engineering" (JTG E20-2019). The index values of technical performances of 70# matrix asphalt are shown in Table 1.

2.1.3 Preparation of light stabilizer-modified asphalt

The preparation process of light stabilizer-modified asphalt is mainly as follows (Figure 2) (Sun *et al.* 2020, 2021): First, place the 70# base asphalt into the oven of 130°C for 2 h of insulation. Pour the molten asphalt into a clean beaker and place it on the oil bath heating device at 160 ± 5°C for insulation. Add the pre-weighed HALS (T622) into the asphalt and stir the mixture at the shear speed of 3,000 rpm for 5 min. Place the prepared light stabilizer-modified asphalt into the oven of 120°C constant temperature to swelling and obtain the sample of light stabilizer-modified asphalt.

Table 1: Technical performance values of 70# matrix asphalt

Test items	Result	Technical requirement
Penetration (0.1 mm)	62.8	60–80
15°C Ductility (cm)	>100	>100
Softening point (°C)	47.6	≥45
Brookfield viscosity (135°C, mPa·s)	509.7	—
Solubility (%)	99.7	≥99.5
Wax content (%)	2.0	≤2.2

2.2 Methodology

2.2.1 Sample preparation method

The samples of physical tests and rheological properties (DSR and BBR) were made according to the "Test Specification for Asphalt and Asphalt Mixtures in Highway Engineering" (JTG E20-2019) and subjected to UV radiation. The samples of micro tests (TG, SEM, AFM, and FTIR) in this study were prepared to the film of 2 mm thick first. The modified asphalt film was subjected to UV aging treatment and then made into samples for experimental tests. For micro-experiment (SEM, AFM, FTIR–TG), the samples were obtained from the surface of film and then were performed tests. The UV aging samples of different tests are shown in Figure 3.

2.2.2 UV aging treatment method

The most unfavorable ultraviolet radiation conditions are taken as the main calculation basis, and the conversion method based on energy conversion is used to convert indoor and outdoor ultraviolet aging time (Formula 1). The annual radiation intensity of sunlight in high-altitude areas is about 7,000 MJ·m^{-2}, with ultraviolet radiation accounting for about 6% of the total amount of sunlight. Therefore, it can be calculated that the average annual intensity of ultraviolet

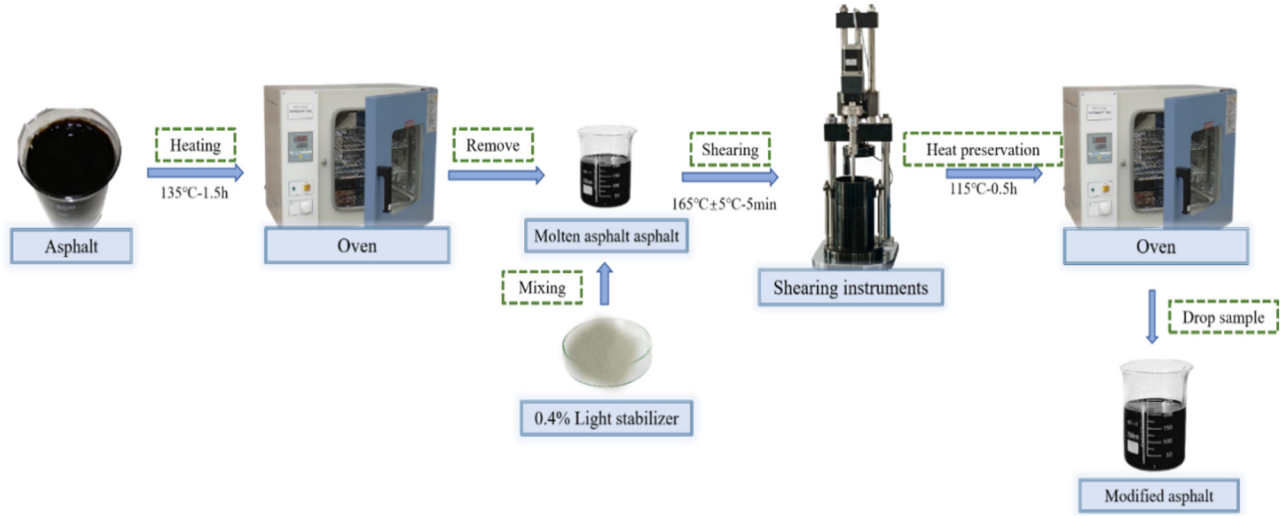

Figure 2: Preparation process of hindered amine light stabilizer-modified asphalt.

radiation is about 420 MJ·m^{-2}. The UV radiant intensity of the artificially accelerated UV light source is about 375 W·m^{-2}, which can convert the artificially accelerated UV aging time to about 305 h. The indoor UV aging equipment is an HD-E802-S UV aging test chamber produced by Haida International Equipment Co., Ltd. The UV radiation intensity was 300 W·m^{-2} and the radiation area was 0.8 m^2.

$$T_{\text{UV-indoor}} = W_{\text{solar}} \times \theta / 3{,}600 W_{\text{indoor}}, \quad (1)$$

where $T_{\text{UV-indoor}}$: indoor UV treatment time (h), W_{solar}: the annual radiation intensity of sunlight in high-altitude areas (MJ·m^{-2}), θ: the rate of ultraviolet radiation accounting for the total amount of sunlight (%), and W_{indoor}: UV radiant intensity of the artificially accelerated UV light source.

2.2.3 X-ray diffraction (XRD) test

The chemical structure of the HALS was characterized by applying the German Bruker D8 ADVANCE X-ray diffraction instrument. The molecular crystal structure information was calculated using the Scheler formula. The experimental

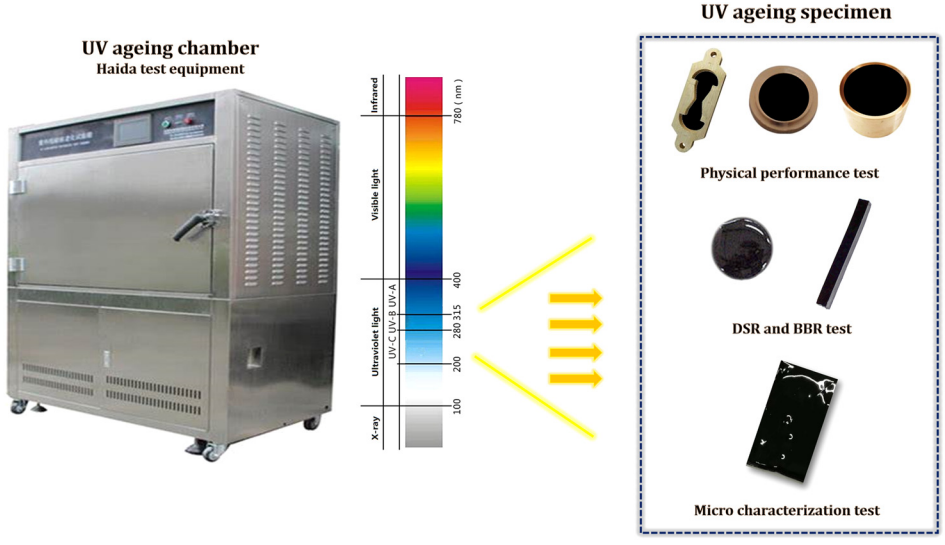

Figure 3: UV aging samples of different tests.

scanning angle range was 1.5–60°, the scanning rate was 5°·min^{-1}, and the step size was 0.02°.

2.2.4 Focused ion beam scanning electron microscopy/energy dispersive X-ray spectroscopy test (FIB-SEM/EDS)

The focused ion beam scanning electron microscopy (FIB-SEM) was used to characterize the micromorphology of the HALS and modified asphalt of different UV aging times. EDS spectroscopy was used to analyze the elemental composition of HALS. The micromorphology magnification included 2,000, 4,000, and 10,000 times.

2.2.5 AFM

The surface roughness of UV-aged modified asphalt was characterized by using the Bruker Dimension FastScan scanning probe microscope. The fast scanning probe was used to scan the micromorphology of the sample surface in ScanAsyst intelligent mode. The instrument probe used was the silicon nitride cantilever probe, and the scanning field sizes were 80 μm × 80 μm.

2.2.6 Thermogravimetric-infrared spectroscopy combined test (FTIR–TG)

The thermal properties and functional group composition of T622 light stabilizer and its modified asphalt were analyzed by using the TG 209 F1 thermogravimetric infrared spectroscopy system produced by NETZSCH in Germany. The infrared spectroscopy test was conducted in the nitrogen atmosphere under the condition of 32 times and the resolution of 4 cm^{-1}. The reaction gas for thermogravimetric analysis was nitrogen, with the purge flow rate of 50 mL·min^{-1}, the heating rate of 10°C·min^{-1}, and the test temperature range of 30–500°C.

2.2.7 Physical and mechanical properties

The penetration, softening point, and ductility tests were carried out in accordance with the "Test Specification for Asphalt and Asphalt Mixtures in Highway Engineering" (JTG E20-2019). The testing temperature for penetration test was 25°C. The ductility test temperature was 15°C and the stretching speed was 5 cm·min^{-1}. The starting temperature of the softening point test was 25°C and the heating rate was 5°C·min^{-1}.

2.2.8 Rheological properties

2.2.8.1 Temperature scanning (TS) test

The TS test adopted strain control mode. The control strain was 12% and the test frequency was 10 rad·s^{-1}. The 25 mm parallel plate was used for testing and the plate spacing was 1 mm. The test temperature range was 46~82°C, and the heating interval was 6°C. At each set temperature, the test was held for 10 min and the shear composite modulus and phase angle values were recorded by every 2 min. Five data points were obtained at each set temperature and the average value was calculated.

2.2.8.2 Rheological test of low-temperature bending beam

According to JTG E20-2019 "Test Specification for Asphalt and Asphalt Mixtures in Highway Engineering" T0627 Asphalt bending creep stiffness test (Bending beam rheometer method), the BBR test was conducted. The BBR test was conducted by using the Cannon TE-BBR bending beam rheometer and the test temperature was −12°C. The creep stiffness S and creep rate m of modified asphalt were tested at 60 s.

3 Results and discussion

3.1 Analysis of physicochemical properties of HALSs

3.1.1 XRD test

The XRD diffraction test results of T622 light stabilizer are shown in Figure 4. From Figure 4, it could be analyzed that the T622 light stabilizer not only has peaks around 15° but also has a certain range of broad peaks after 30°. This indicated that the structure of T622 HALS coexisted with crystalline and amorphous structures. According to the calculation of crystallinity and Xie Le formula, its crystallinity is about 64.22%.

3.1.2 FIB-SEM/EDS

At the magnification of 2,000 times (Figure 5a), the T622 light stabilizer mainly consists of circular structures. In addition to the elliptical structures of similar sizes, there are a small number of rod-shaped structures and larger

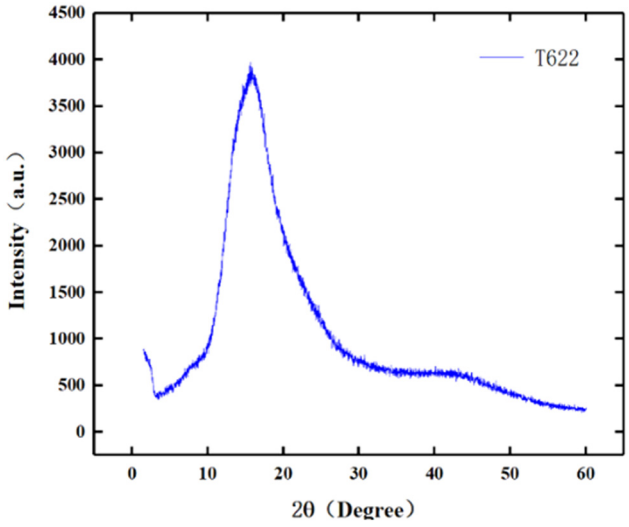

Figure 4: XRD test results of T622.

elliptical structures. When the complete elliptical structure in the characterization results is further magnified to 5,000 times (Figure 5b), it could be observed that the surface of the ellipse is relatively smooth. There are a small number of horizontally distributed cracks in the middle, and one of the open cracks partially displays its internal structure. There are vertical cracks on the left edge, which has the color difference between the structural edge and inside part. This might be due to the height difference between the edge structure and the internal structure, resulting in uneven color distribution in the electron microscopy characterization results, which indicates that the surface of the T622 structure has certain high and low fluctuations and roughness. Under 10,000 times magnification (Figure 5c), there are many cracks, grooves, potholes, and layers on the surface, resulting in the more complex structural on T622 particle surface. Figure 5d and e shows the distribution of the two elements with the highest content, verifying that the key elements of T622 light stabilizer are mainly C and O. The distribution of these two elements in the structure is basically consistent with the position of the microstructure, which are distributed on both the surface and plane of the structure.

3.1.3 TG test

From the analysis of the thermogravimetric curve in Figure 6, it could be known that the T622 light stabilizer begins to decompose when the temperature rises to 205°C. Meanwhile, the DTG curve shows that the T622 light stabilizer exhibits the maximum weight loss peak at 357°C. At 407°C, the residual mass of T622 light stabilizer is only 0.78%, almost completely decomposed,

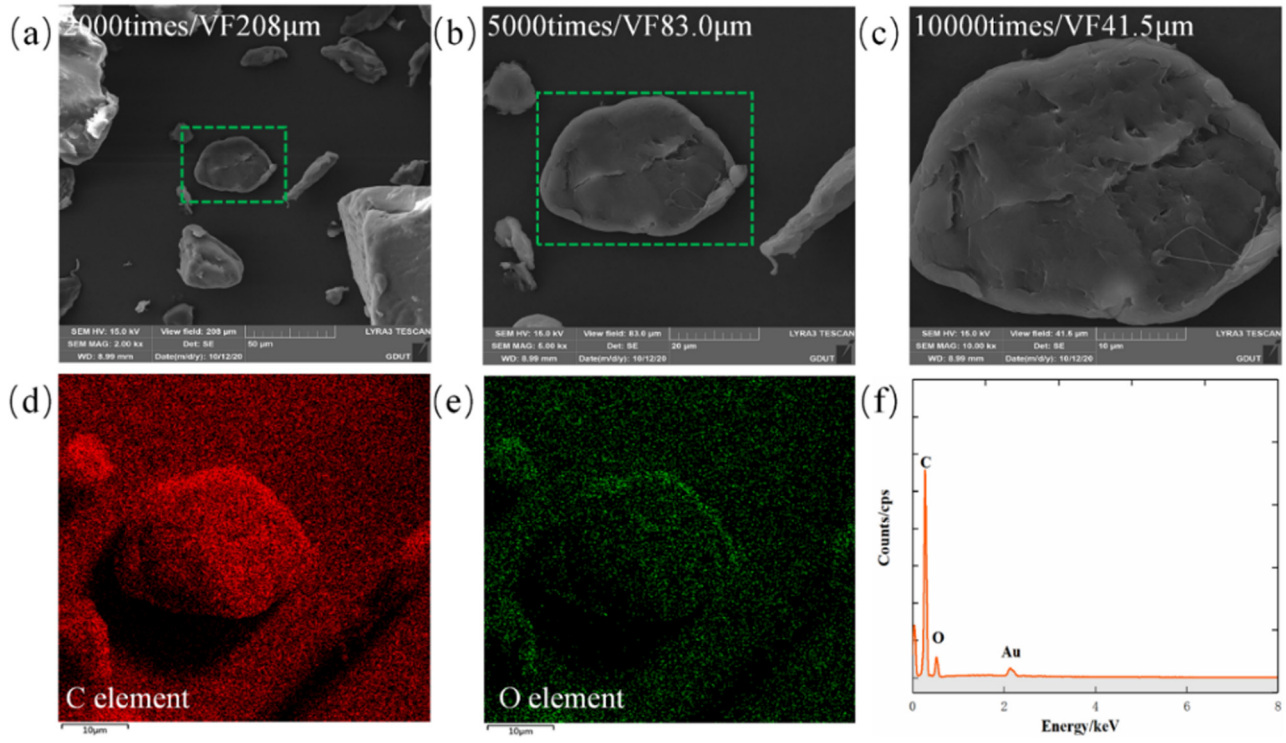

Figure 5: Micromorphology and element composition results of T622. (a) SEM-2000 times; (b) SEM-5000 times; (c) SEM-10000 times; (d) EDS-C element; (e) EDS-O element and (f) EDS result.

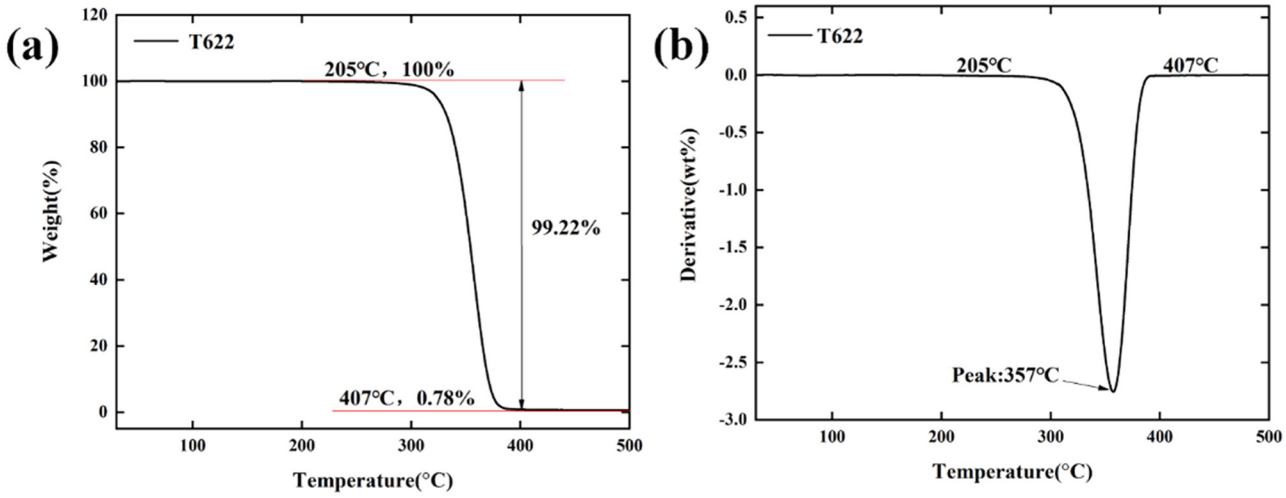

Figure 6: Thermogravimetric analysis results of T622 light stabilizer. (a) TG and (b) DTG.

Table 2: Pyrolysis characteristic values of T622 light stabilizer

Modifier	$T_{initial}$/°C	T_{end}/°C	T_{max}/°C	Residual rate/%
T622	205	407	357	0.78

and the pyrolysis reaction has basically ended. Afterwards, as the temperature continues increasing to the ending temperature of 500°C, the weight change of T622 light stabilizer is almost zero. According to the pyrolysis curve and Table 2, the initial decomposition temperature of T622 light stabilizer is 205°C. According to the DTG curve, as the temperature increases, the decomposition rate of T622 light stabilizer is faster. The temperature corresponding to the maximum weight loss rate is 357°C. Under the influence of high temperature, the internal structural chain breaks, and almost all the materials undergo pyrolysis. The remaining might be residual carbon materials that could not be further decomposed.

3.1.4 Dynamic FTIR test

From Figure 7, it could be analyzed that the T622 light stabilizer is always in the stable stage during the first 28 min of dynamic heating, indicating that there is little detection of material production during this time period, and the intensity is almost at the zero scale position. Afterwards, as the temperature increases, the strength curve begins to change. The infrared spectra of three characteristic time points are obtained for analysis, namely 29.28 min when the intensity began to change, 33.36 min when the intensity reached its maximum value, and 39.32 min when the intensity decreased to its minimum value. At 29.28 min, substances are produced and the intensity of the G–S curve begins to change. Multiple characteristic peaks with lower intensity could be identified through spectral analysis, with 1809.86 and 1044.18 cm^{-1} being the C═O bond stretching vibration of anhydride and the C–O bond of saturated fatty anhydride, respectively. As the temperature continues to rise, it reaches the maximum intensity at 33.36 min, and the characteristic peak intensity in the spectrogram increases significantly. A total of 2974.58 cm^{-1} represents the characteristic peak of methyl group, and the two characteristic peaks appearing in the range of 1751.17 and 1,050–1,300 cm^{-1} are the C═O bond stretching vibration absorption of ester group. When the time reaches 39.32 min, the strength curve has already tended to be flatten out. At the same time, the absorption peak in the spectral curve decreases and the position of its characteristic peak remains unchanged.

3.2 Microscopic morphology evolution of light stabilizer-modified asphalt

3.2.1 SEM test

3.2.1.1 Matrix asphalt

Figure 8 shows the characterization results of the UV-induced microstructure of matrix asphalt with different scanning times. From Figure 6a and b, it could be observed that after 76.25 h UV aging treatment, there are obvious aggregated parallel cracks (marked in yellow) on the surface of asphalt, and there are locally closed like fragmentation areas (marked in red). After zooming in 500 times

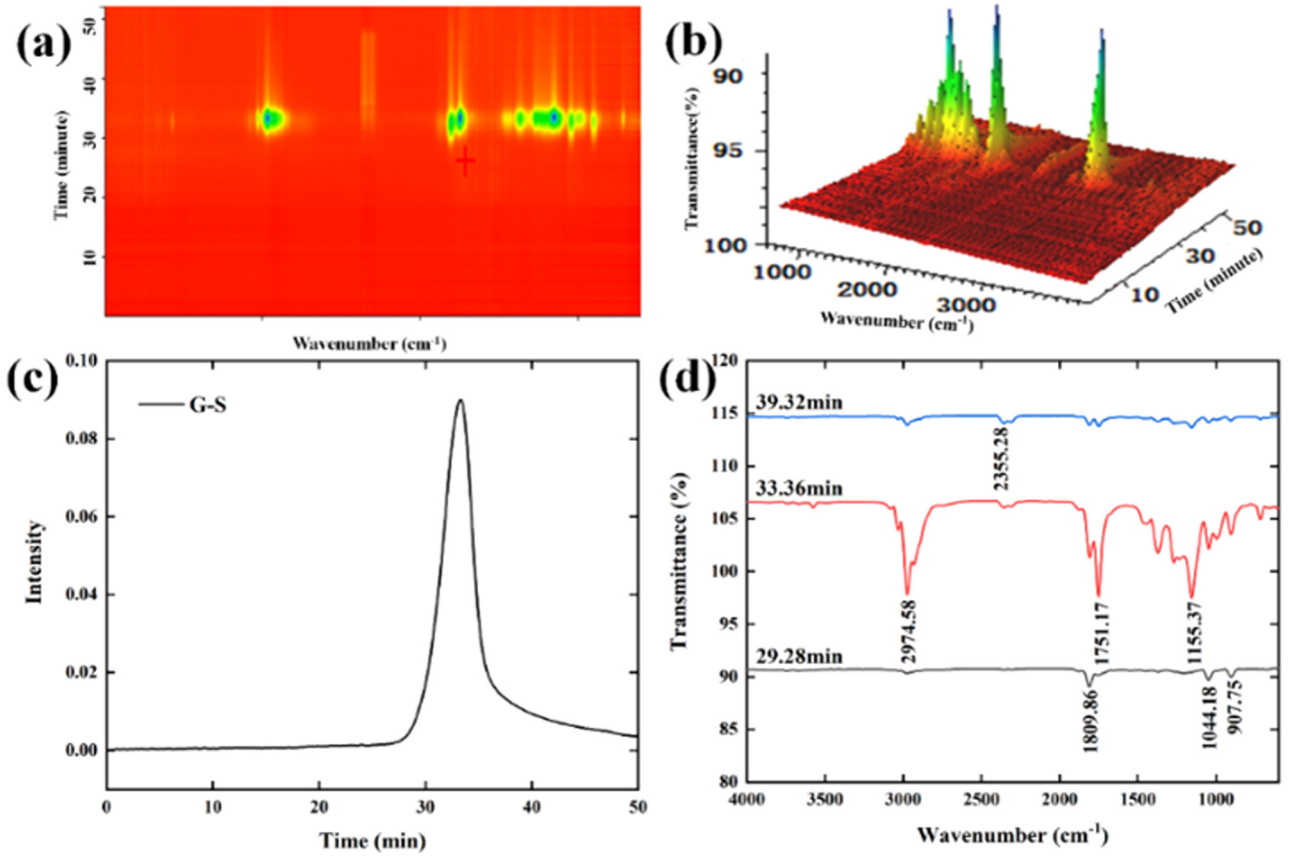

Figure 7: Infrared spectral analysis results of T622 light stabilizer. (a) 2D result; (b) 3D result; (c) Intensity and (d) Transmittance.

(Figure 8c), it is found that the middle of the crack mostly presents the straight line shape, while both ends show the certain angle of deflection. There is no trend of interconnectivity or continuity between different cracks. However, when further amplification to 1,000 times (Figure 8c) and 2,000 times (Figure 8e), it could be confirmed that there is no connection between cracks, which had independent forms instead of connections. When the UV aging time is extended to 152.5 h, it could be observed from Figure 8f that a series of closed blocks appear on the asphalt surface, and there is a clear shared boundary between these blocks. After amplifying on the partially closed block (Figure 8g), it could be found that the boundary of the block evolved into the banded protrusion instead of crack. After further amplification of the boundary, the morphology of the protruding structure could be clearly observed, which has a certain height difference compared to the surrounding flat area that is mostly in the striped state. This is very similar to the crack morphology that occurred at 75.25 h, possibly due to the increasing temperature of asphalt after absorbing ultraviolet radiation energy, which causes asphalt flowing and filling the crack area to form the convex structure.

When the UV aging time reaches 228 h, it can be observed from Figure 8k that dense parallel cracks appear again on the asphalt surface. Different from 76.25 h, there are also vertical cracks intersecting parallel cracks on the surface of UV-aged asphalt at 228 h. This causes parallel cracks to connect with each other, leading to the appearance of closed cracks and blocky fragments. The cracks amplified to 1,000 times and 2,000 times (Figure 8l and m) reveal the presence of vertical crack connections between different parallel cracks and the appearance of obvious closed cracks, most of which are rectangular structures. After further amplifying the rectangular structure (Figure 8n and o), the circular structure with the diameter of approximately 1.5 μm is identified inside it. When the UV aging time reaches 305 h, it can be observed from Figure 8p–r that the closed cracks on the asphalt surface disappear, mainly appearing as parallel cracks. At the same time, the density and number of cracks significantly decreased. After locally enlarging the cracks to 4,000 and 8,000 times (Figure 8s and t), it is found that circular protrusions and holes of different diameters appear in the surrounding areas of the cracks.

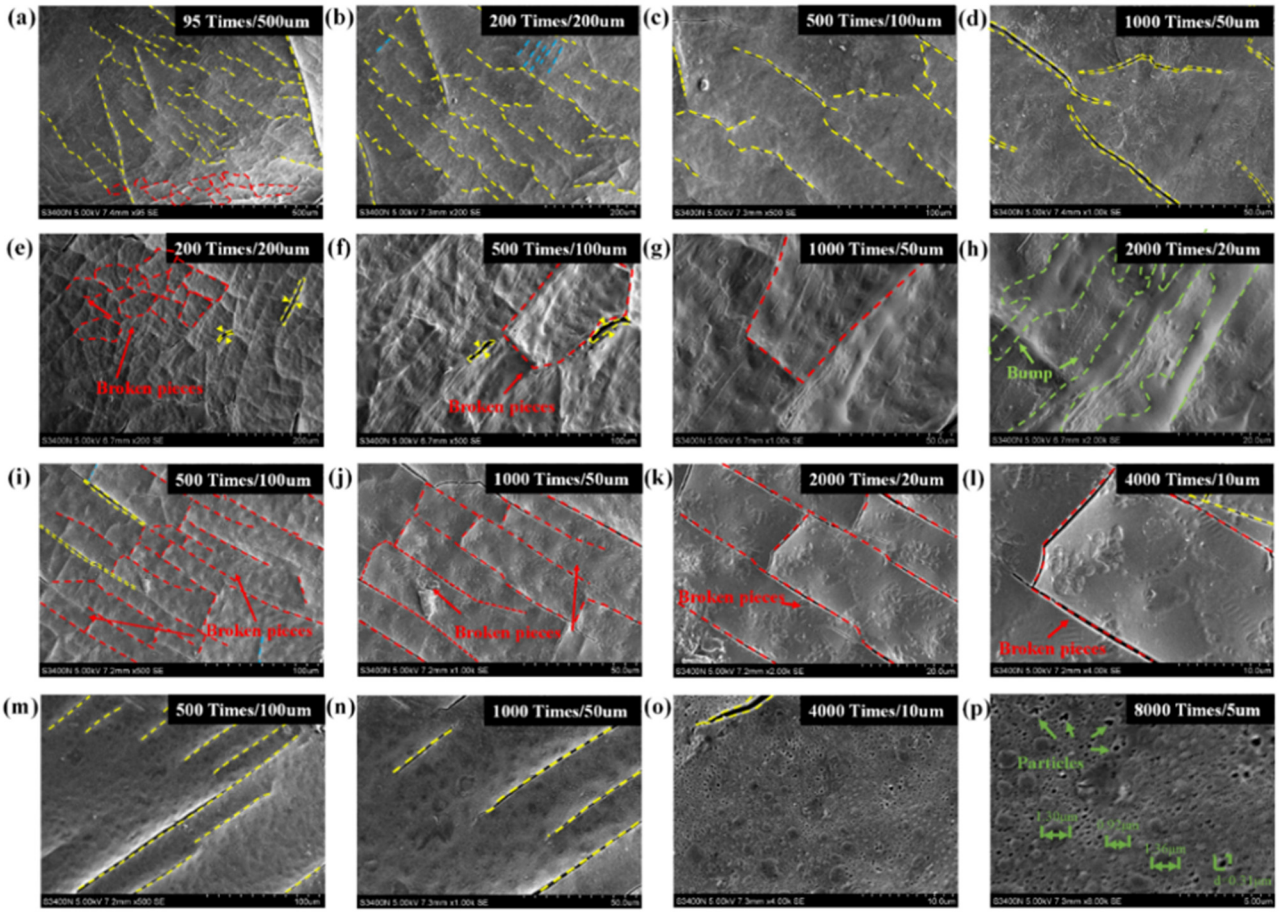

Figure 8: Ultraviolet-induced microscopic morphology of matrix asphalt. (a) 76.25 h–95 times; (b) 76.25 h–200 times; (c) 76.25 h–500 times; (d) 76.25 h–1000 times; (e) 152.5 h–200 times; (f) 152.5 h–500 times; (g) 152.5 h–1000 times; (h) 152.5 h–2000 times; (i) 225 h–500 times; (j) 225 h–1000 times; (k) 225 h–2000 times; (l) 225 h–4000 times; (m) 305 h–500 times; (n) 305 h–1000 times; (o) 305 h–4000 times and (p) 305h–8000 times.

3.2.1.2 T622 light stabilizer-modified asphalt

Figure 9 shows the microstructure of T622 light stabilizer-modified asphalt at different UV stages. From the microstructure of the asphalt surface aged for 76.25 h in Figure 9a, it could be seen that there is the valley-shaped "fold structure" in the micro area of the asphalt surface. The structural form presents the micromorphology of depression in the middle and protrusions around it (marked in yellow), whose width ranged approximately from 9.21 to 33.51 μm. At the magnification of 2,000 times (Figure 9d), it could be observed that there are irregular protrusions in the interval area of the fold structure. As the UV aging time prolongs, the protruding structures gradually aggregate. The edges of the structure tend to be smooth, and there are no obvious wrinkles on the asphalt surface within the characterization area. The UV aging time is extended by 152.25 h, and it can be observed from Figure 9k that the connection between fold structures is closer and there is obvious trend of interconnectivity between structures. Further amplified to 2,000 times (Figure 9i) and 4,000 times (Figure 9j), the boundaries formed by the folded structure gradually blur, the structure sinks in and begins to merge with adjacent structures, gradually transforming into parallel "crack structures." From Figure 7n and o, it can be seen that when the UV aging time is extended to 228 h, the initial crack structure formed on the asphalt surface transforms into the long strip like "ridge" structure similar to the fold structure and gradually evolves into the tightly connected fold structure. As the UV aging process deepens, the density of fold structures increases significantly and is parallel to each other, resulting in a narrow and elongated overall structure. After UV aging for 305 h (Figure 9p), the typical morphology changes from the original parallel state "fold structure" to the potential cross-state "network" structure. The structure presents the irregular block shape, but the smooth area between the structures increases without obvious crack boundaries. This indicates that long-term UV aging has the significant impact on the surface morphology of asphalt, forming potential fragmented block-shaped areas.

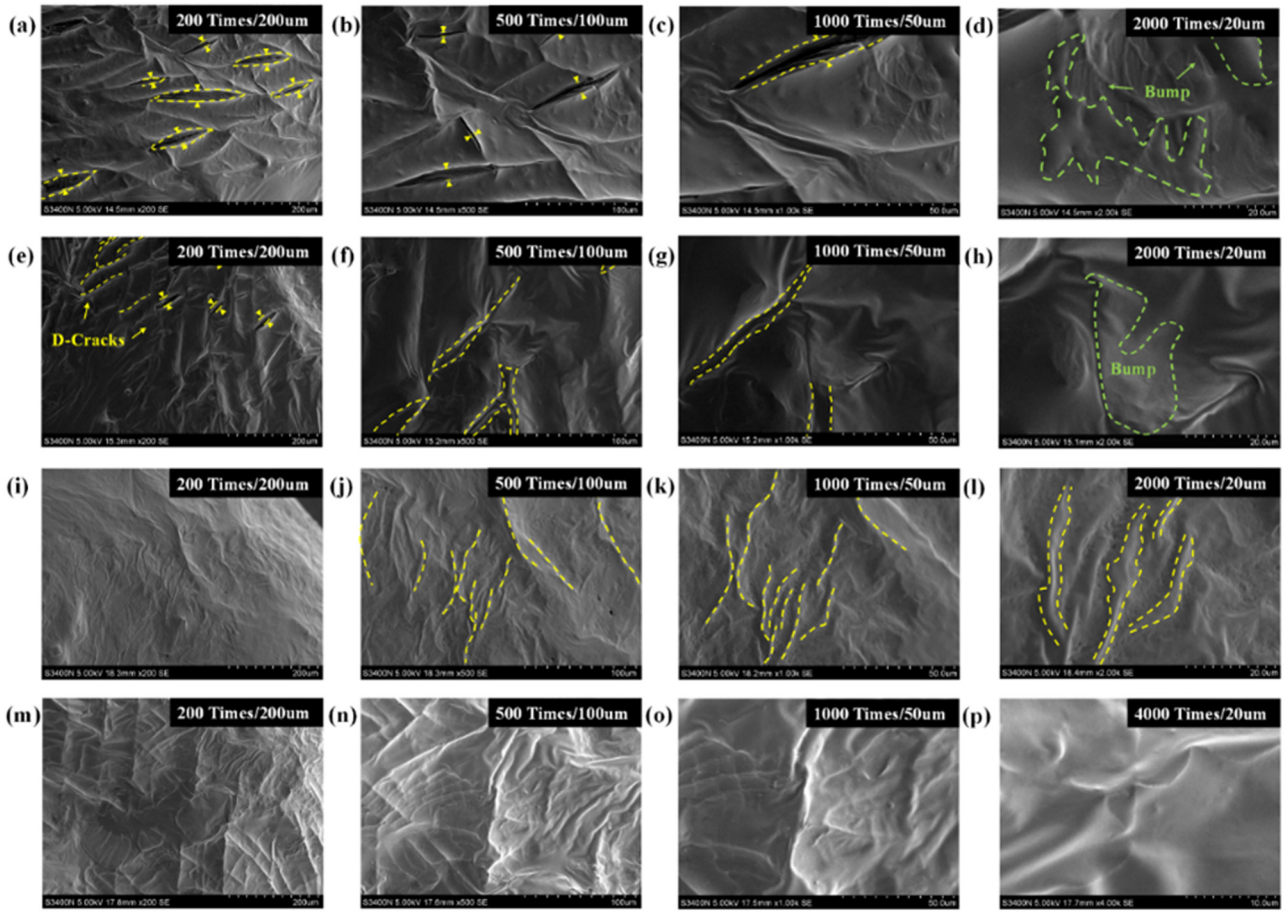

Figure 9: SEM morphology of T622 light stabilizer-modified asphalt. (a) 76.25 h–200 times; (b) 76.25 h–500 times; (c) 76.25 h–1000 times; (d) 76.25 h–2000 times; (e) 152.5 h–200 times; (f) 152.5 h–500 times; (g) 152.5 h–1000 times; (h) 152.5 h–2000 times; (i) 225 h–200 times; (j) 225 h–500 times; (k) 225 h–1000 times; (l) 225 h–2000 times; (m) 305 h–200 times; (n) 305 h–500 times; (o) 305 h–1000 times and (p) 305 h–4000 times.

3.2.2 AFM test

3.2.2.1 Matrix asphalt

Figures 10–11 show the AFM characterization results of matrix asphalt under different UV aging times. It is found from the AFM results that the roughness change of the base asphalt results in the obvious bright and dark domain zoning in the 2D morphology, and the granular structure is evenly dispersed in the figure, with the overall surface tending to be flat. In Figure 10b, there is a clear clustering region boundary between the bright and dark domains, indicating that as the UV aging process progresses, the

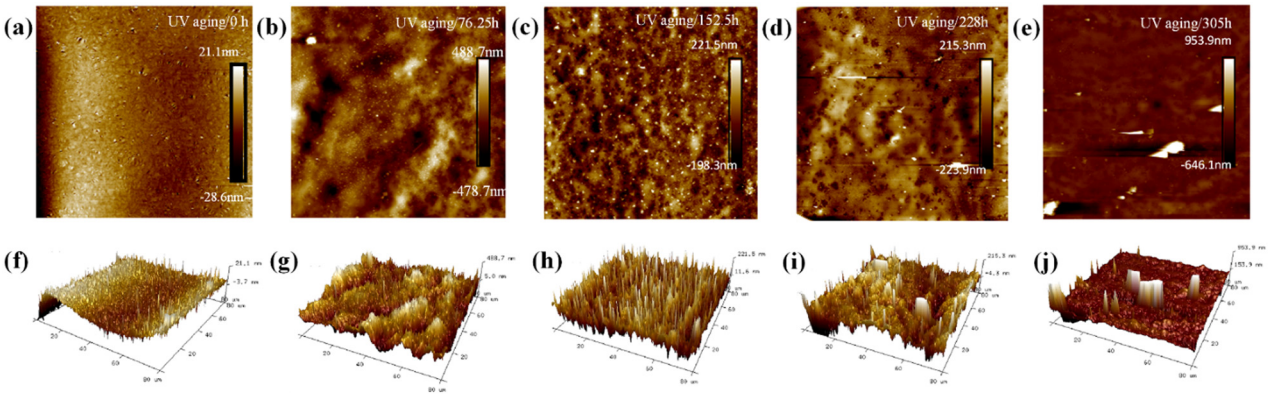

Figure 10: AFM characterization results and grayscale processing of matrix asphalt at different UV aging times. (a) 0 h-2D; (b) 76.25 h-2D; (c) 152.5 h-2D; (d) 228 h-2D; (e) 305 h-2D; (f) 0 h-2D; (g) 76.25 h-3D; (h) 152.5 h-3D; (i) 228 h-3D and (j) 305 h-3D.

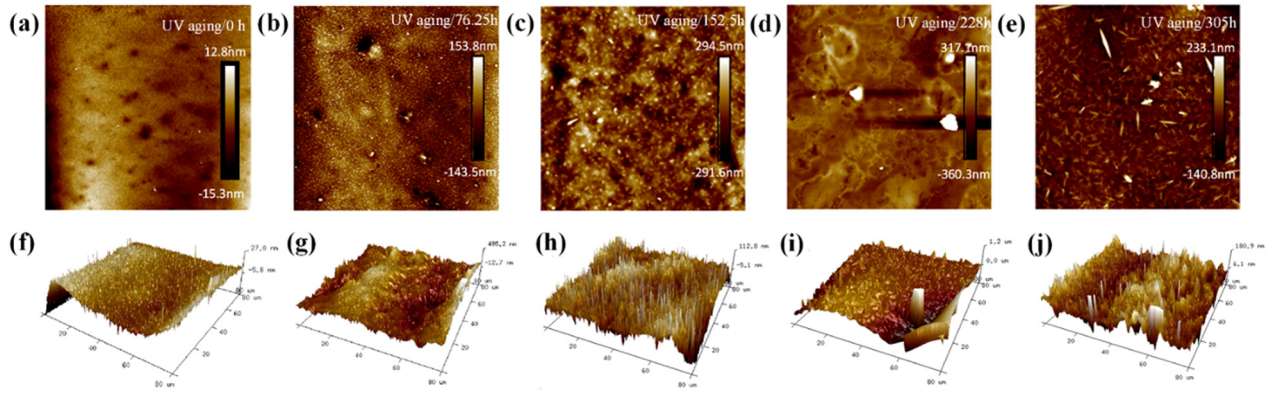

Figure 11: AFM characterization results and grayscale processing of T622-modified asphalt at different UV aging times. (a) 0 h-2D; (b) 76.25 h-2D; (c) 152.5 h-2D; (d) 228 h-2D; (e) 305 h-2D; (f) 0h-2D; (g) 76.25 h-3D; (h) 152.5 h-3D; (i) 228 h-3D and (j) 305 h-3D.

overall morphology of asphalt gradually becomes more complex, which is also gradually reflected in subsequent Figure 10c and d. As the UV aging time continues to extend, the distribution of bright regions gradually concentrates, and the boundary between bright and dark regions in Figure 11d becomes more obvious. In the 3D analysis results, the changes in surface morphology are more significant. The total height of the aged matrix asphalt surface in Figure 11b decreases, manifested as the uniformly distributed "needle-like structure" in the 3D morphology. When the aging time reaches 228 h, the area of the bright region begins to concentrate, and a large diameter aggregated "columnar structure" appears in Figure 11d. When the UV aging time reaches 305 h, the bright regions in Figure 10e are highly concentrated, and there is a clear aggregation convex structure on the surface of the matrix asphalt in the 3D morphology image.

3.2.2.2 T622 light stabilizer-modified asphalt

Figure 11 shows the AFM characterization results of T622 light stabilizer-modified asphalt under different UV aging times. According to Figure 11b, when the UV aging time is 76.25 h, the boundary between the bright and dark areas on the surface is not obvious and the distribution of light and dark is mixed. According to the analysis in Figure 11c and h, when the UV aging time reaches 152.5 h, the micro surface height distribution of modified asphalt is uniform and the fluctuation and protrusion structures are reduced. When the aging time reaches 305 h, the asphalt surface exhibits the bright and dark color distribution once again, presenting complex morphologies such as peaks and valleys.

3.3 Thermophysical properties and functional group composition of light stabilizer-modified asphalt

3.3.1 TG test

3.3.1.1 Matrix asphalt

According to Figure 12 and Table 3, the initial decomposition temperature of 70# asphalt decreases from 232.6°C for 76.25 h to 158.8°C for 305 h. Under the influence of prolonged UV aging time, the significant decrease in initial decomposition temperature leads to the later thermal decomposition of asphalt at lower temperatures. The difference in decomposition temperature between the beginning and ending of aged asphalt reached 73.8°C, and the decrease in decomposition temperature indicates that the anti UV aging performance of the asphalt stays in the low level without modification. At the ending temperature, the residual weight rate of asphalt remains around 20%, indicating that the remaining portion is relatively stable and not directly related to the duration of ultraviolet light exposure.

3.3.1.2 T622 light stabilizer-modified asphalt

From Figure 13 and Table 4, it can be seen that with the extension of UV aging time, the initial weight loss temperature of T622 light stabilizer-modified asphalt gradually decreases from 180.2 to 172.9°C, with the temperature difference of about 7.3°C, which is much lower than the 73.8°C of 70# asphalt. This indicates that the addition of HALSs alleviates the impact of ultraviolet radiation effectively on the thermal properties of asphalt. The increase in initial decomposition temperature of modified asphalt is related

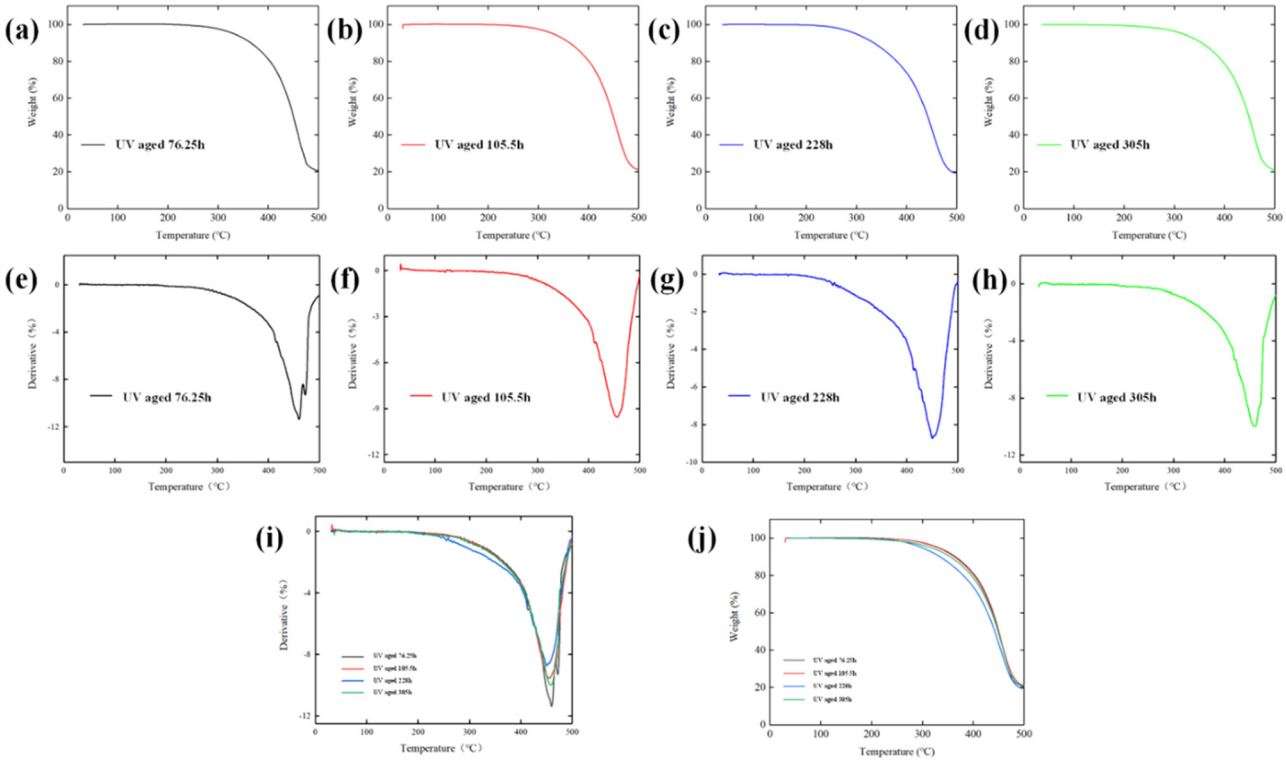

Figure 12: Thermogravimetric curves of 70# matrix asphalt under different UV aging times. (a) 76.25 h-TG; (b) 152.5 h-TG; (c) 228 h-TG; (d) 305 h-TG; (e) 76.25 h-DTG; (f) 152.5 h-DTG; (g) 228 h-DTG; (h) 305 h-DTG; (i) Comparison-TG and (j) Comparison-DTG.

to the extension of aging time, which leads to the volatilization and migration of light components, thereby affecting the changes in thermal properties of asphalt. According to the DTG curve analysis, the T622 light stabilizer-modified asphalt corresponding to the four aging time points shows the maximum weight loss rate in sequence within 450–460°C. The temperature difference between the front and rear remained around 3°C and dropped to the lowest point of all aging times at the temperature corresponding to the weight loss rate at the final aging time. This indicates that T622 light stabilizer-modified asphalt would undergo early weight loss decomposition after long-term UV aging. The gradual decrease in the final residual rate indicates that the extension of UV aging time affects the final quality loss of T622 light stabilizer-modified asphalt.

3.3.2 FTIR test

3.3.2.1 Matrix asphalt

From Figure 14, it could be analyzed that the strong absorption peaks generated by 70# matrix asphalt under ultraviolet radiation range from 2,800 to 3,000 cm^{-1}, and the absorption peaks in this range are mainly caused by the stretching vibration peaks of methylene and methyl. In addition, there are intermediate strength carbonyl functional groups at the wavenumber position of 1,700 cm^{-1}, which are generated due to the reaction of internal components of asphalt caused by temperature rise during the experiment, such as carbonyl groups generated by oxygen absorption reaction. The sulfoxide group is produced by the reaction of asphalt-containing sulfides. As the temperature

Table 3: Thermogravimetric index of 70# asphalt under different UV aging times

Aging time (h)	Initial decomposition temperature (°C)	Temperature corresponding to maximum weight loss rate (°C)	Weight loss rate (%)
76.25	232.6	459.6	77.51
152.5	226.6	455.1	78.76
228	200.7	450	80.63
305	158.8	447.6	81.04

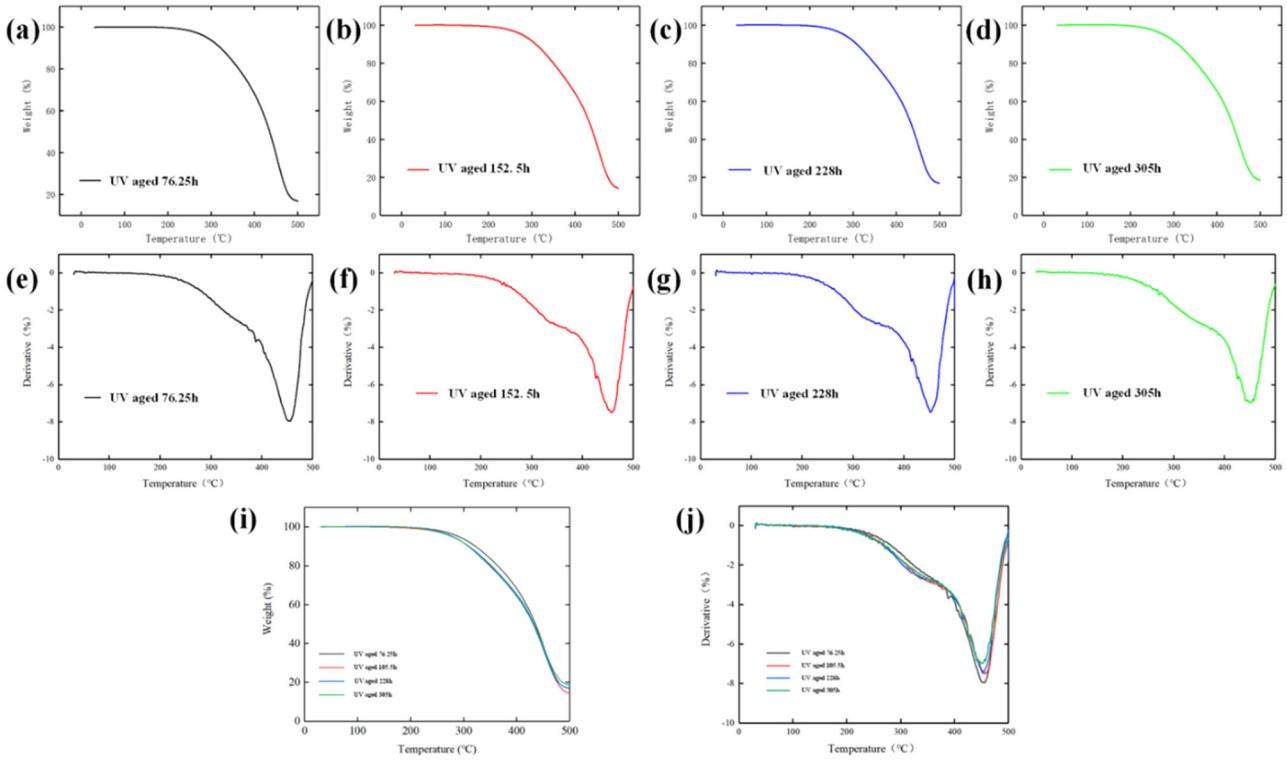

Figure 13: Thermogravimetric curves of T622-modified asphalt under different UV aging times. (a) 76.25 h-TG; (b) 152.5 h-TG; (c) 228 h-TG; (d) 305 h-TG; (e) 76.25 h-DTG; (f) 152.5 h-DTG; (g) 228 h-DTG; (h) 305 h-DTG; (i) Comparison-TG and (j) Comparison-DTG.

increases, the reaction rate of the matrix asphalt also changes accordingly.

From Figure 15, it could be known that the extension of UV aging time is not significantly related to the time when the matrix asphalt product begins to form but corresponds to the temperature at which reaches its peak. As the UV aging time prolongs, the characteristic peak temperature gradually increases, but the increase rate is relatively slow, increasing by about 10°C throughout the entire UV aging cycle. When prolonged ultraviolet radiation for 228 and 305 h, the absorption peak intensity in the region increases at around 1,500 cm^{-1}. This indicates that there is a significant difference in the functional groups generated during this period compared to before, which might be due to the UV aging extension of asphalt binder.

Due to the differences in the spectra of 70# matrix asphalt after aging compared to light stabilizer-modified asphalt, it is necessary to redefine the quantitative calculation formula for the spectra of 70# matrix asphalt. The index $\sum A$ is defined as follows:

$$\sum A = A_{1700} + A_{1601} + A_{1456} + A_{1377} + A_{1300} + A_{1030} + A_{902} + A_{746}. \quad (2)$$

According to the analysis of exponential growth of functional groups in Table 5 and Figure 16, under the action of 228–305 h ultraviolet radiation, the aging degree of matrix asphalt without HALS is significantly greater than that at the first two time points. After UV aging, the functional group exponential growth of 70# matrix asphalt increases by 7.82 times for the carbonyl group, 8.07 times

Table 4: Thermogravimetric index of T622-modified asphalt under different UV aging times

Aging time	Initial decomposition temperature (°C)	Temperature corresponding to maximum weight loss rate (°C)	Weight loss rate (%)
76.25 h	180.2	449.5	81.4
152.5 h	178.8	456.9	82.6
228 h	177.1	455.0	83.0
305 h	172.9	453.1	83.0

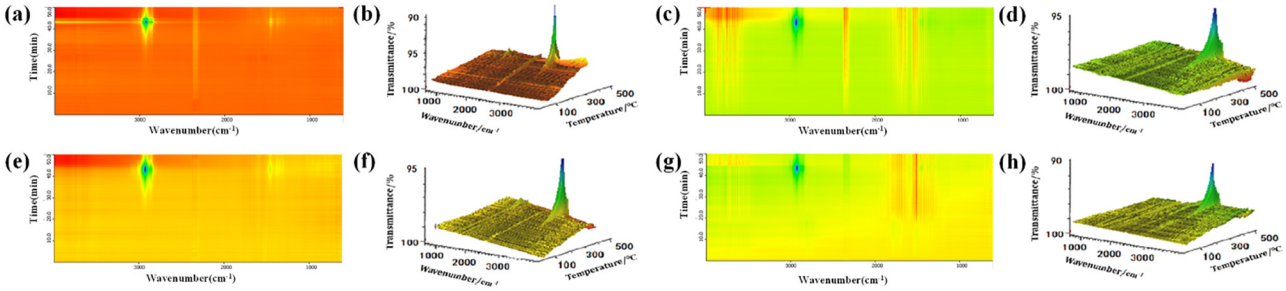

Figure 14: 3D and 2D infrared spectra of 70# matrix asphalt under different UV aging times. (a) 76.25 h-2D; (b) 76.25 h-3D; (c) 152.5 h-2D; (d) 152.5 h-3D; (e) 228 h-2D; (f) 228 h-3D; (g) 305 h-2D and (h) 305 h-3D.

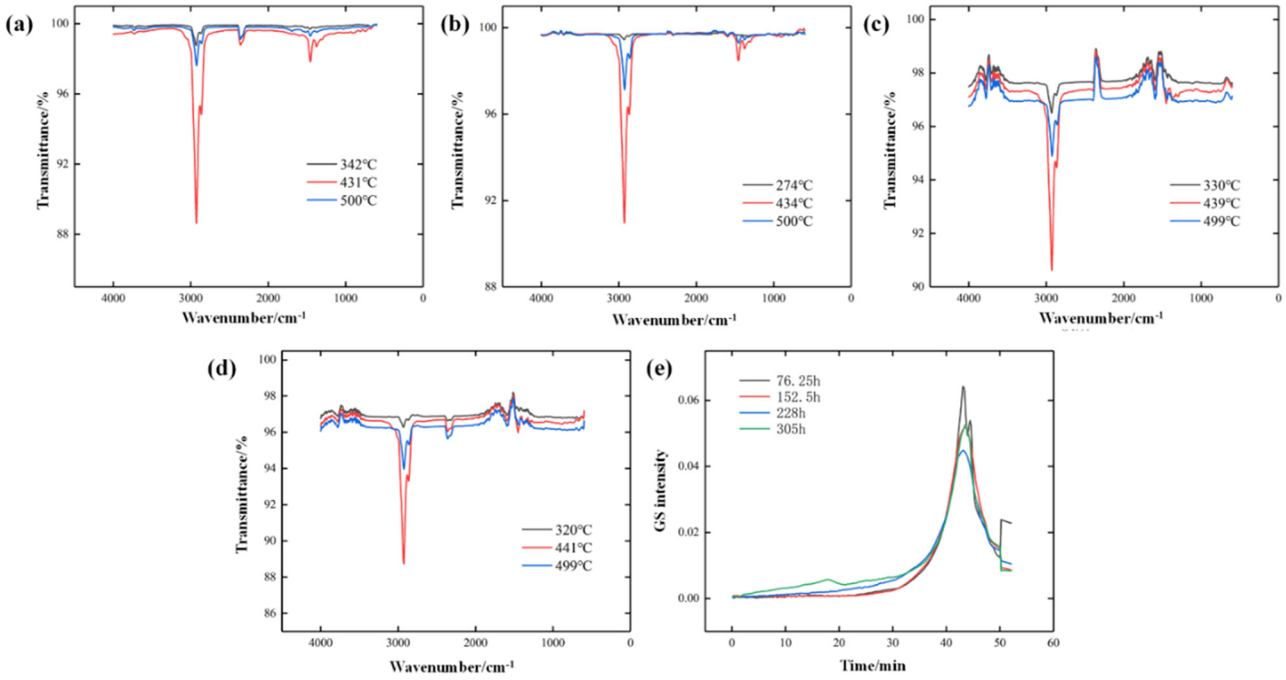

Figure 15: Infrared spectra of 70# matrix asphalt under different UV aging times. (a) 76.25 h; (b) 152.5 h; (c) 228 h; (d) 305 h and (e) GS intensity.

for the sulfoxide group, and 5.94 times for the aromatic functional group. The exponential growth of the carbonyl group and the sulfoxide group increases significantly, indicating that the matrix asphalt has experienced obvious aging after a long time of ultraviolet radiation, and the ultraviolet aging destroys the colloidal structural stability inside asphalt.

3.3.2.2 T622 light stabilizer-modified asphalt

From Figures 17 and 18, it could be shown that the infrared spectrum of T622 light stabilizer-modified asphalt shows almost no changes in the first 20 min (i.e., 230°C), with the difference only manifested in the initial reaction time. After 10 min gentle period, the reaction begins to occur around 30 min. The degree of reaction increases gradually with time, reaching its maximum peak around 43 min, corresponding to 435°C in the spectrogram. The strong absorption peak and the shoulder peak of 2,860 cm^{-1} appear at 2,920 cm^{-1}, specifically the asymmetric and symmetric stretching vibration peaks of C–H in methylene –CH_2–. The absorption peak of about 1,457 cm^{-1} is a shear vibration of methylene –CH_2–.

Table 5: Aging index of characteristic functional groups of 70# matrix asphalt

Aging time (h)	Index of characteristic functional groups		
	$I_{C=O}$	I_{Ar}	$I_{S=O}$
76.25	0.0832	0.1181	0.1181
152.5	0.0354	0.0887	0.0752
228	0.3526	0.6135	0.6718
305	0.7338	1.0716	0.8194

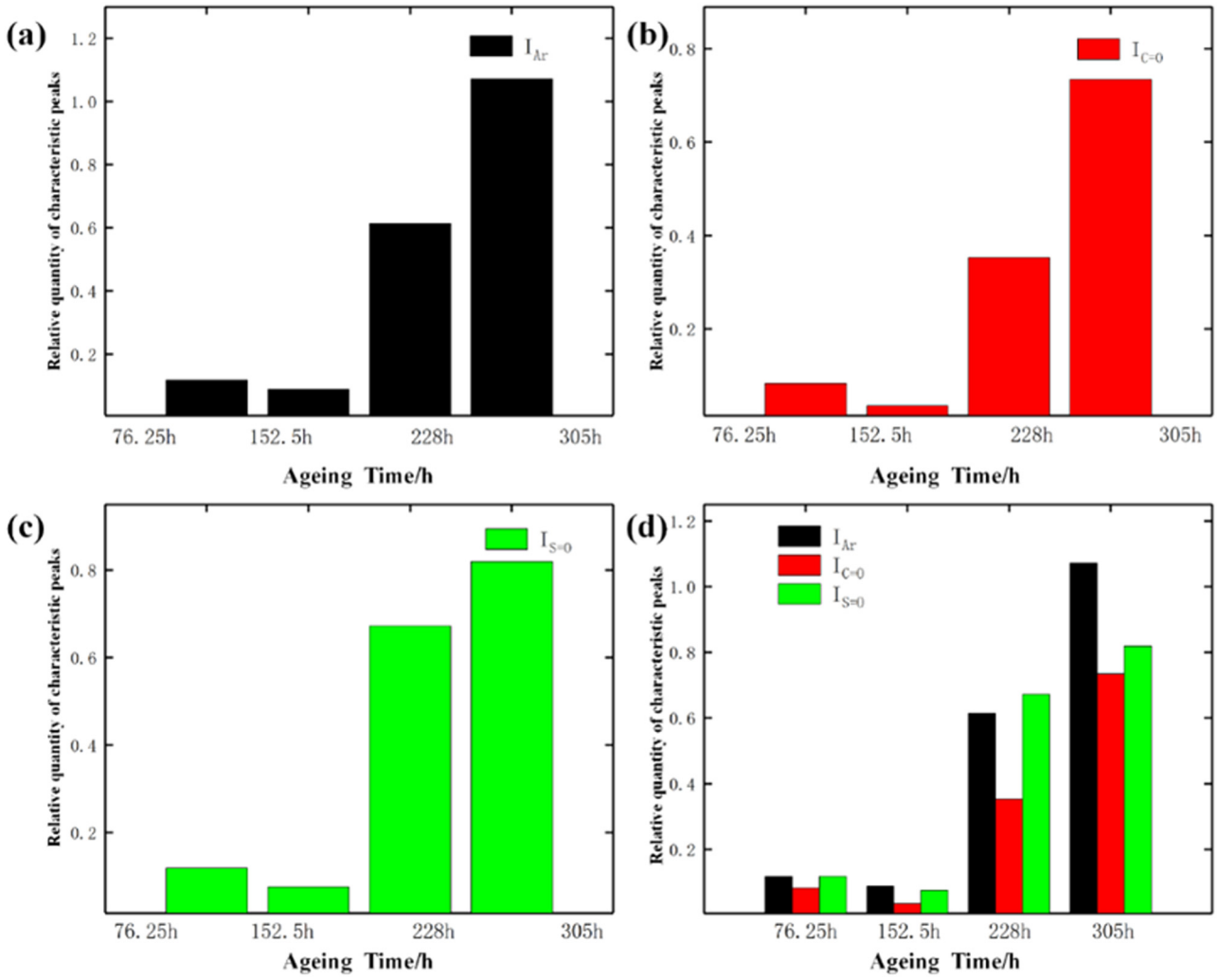

Figure 16: Aging index variation of characteristic functional groups of 70# matrix asphalt. (a) I_{Ar}; (b) $I_{C=O}$; (c) $I_{S=O}$ and (d) Comparision.

According to the analysis in Figures 17 and 18, the functional group composition in the asphalt after UV aging listed is basically consistent. The main difference is due to the difference of aging time. This indicates that under the modification effect of light stabilizers, asphalt could still exhibit good performance when suffering from different times of ultraviolet irradiation. The quantitative calculation of $\sum A$ in the spectrum of T622 light stabilizer-modified asphalt is redefined as follows:

$$\sum A = A_{1700} + A_{1644} + A_{1601} + A_{1550} + A_{1456} + A_{1377} + A_{1200} + A_{1141} + A_{1100} + A_{1030} + A_{890} + A_{744}. \quad (3)$$

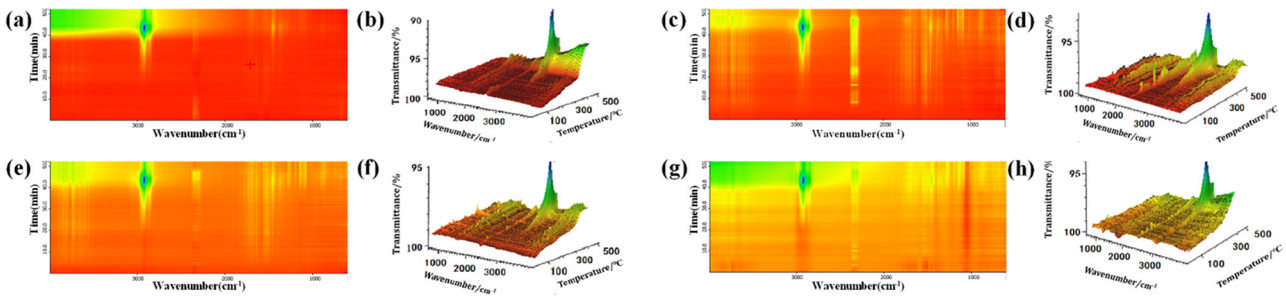

Figure 17: 3D and 2D infrared spectra of T622-modified asphalt under different UV aging times. (a) 76.25 h-2D; (b) 76.25 h-3D; (c) 152.5 h-2D; (d) 152.5 h-3D; (e) 228 h-2D; (f) 228 h-3D; (g) 305 h-2D and (h) 305 h-3D.

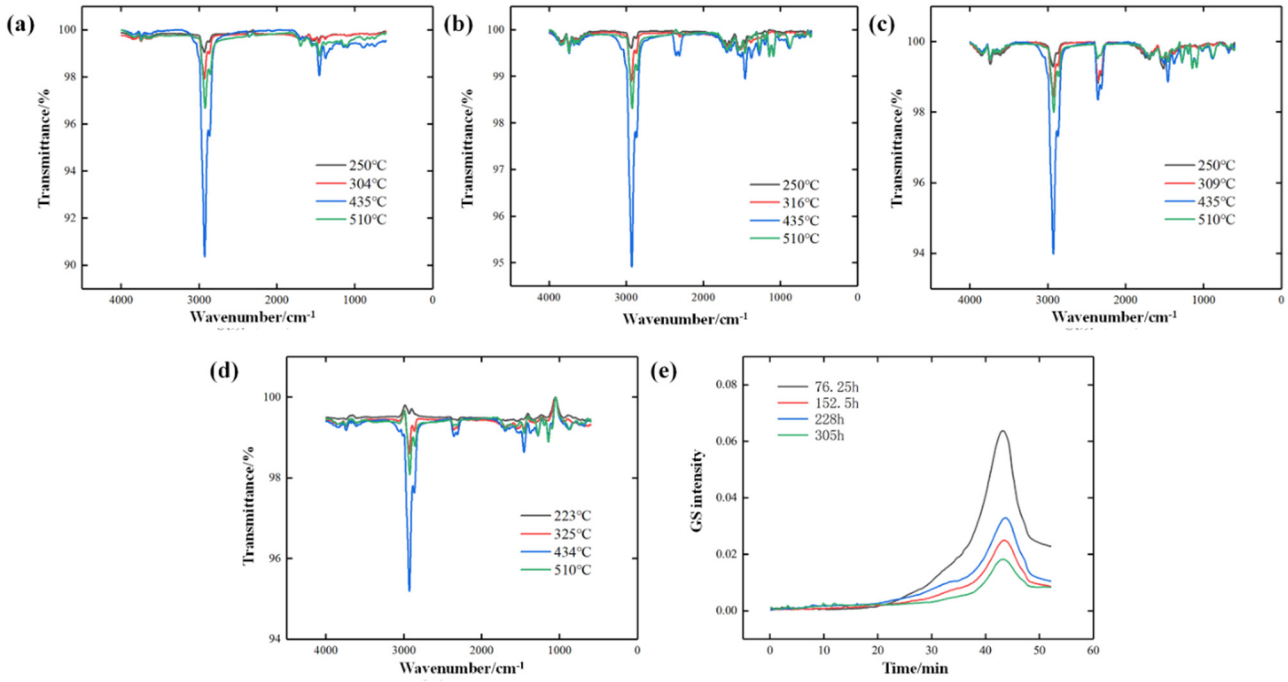

Figure 18: Infrared spectra of T622-modified asphalt under different UV aging times. (a) 76.25 h; (b) 152.5 h; (c) 228 h; (d) 305 h and (e) GS intensity.

From Table 6 and Figure 19, it could be analyzed that with the extension of UV radiation time, there is a significant increase in aromatic functional groups and carbonyl index, with a more significant increase in the range of 76.25–152.5 h. This indicates that the aging of T622 asphalt during this period is relatively affected by ultraviolet radiation, which accelerates the transformation of internal components in asphalt. After 152.5 h, the increase in UV aging index becomes relatively slow, and the aromatic functional groups also decreased to the certain extent. For the sulfoxide group, the index remains at a high level at 76.25 h of the early stage of UV aging and at 305 h of the end of UV aging, while it is relatively low at the intermediate time points of 152.5 and 228 h. Although T622 light stabilizer-modified asphalt would still produce corresponding functional groups under the influence of ultraviolet radiation, the growth rate and exponential growth amount of relevant functional map are significantly lower than that of base asphalt. This also shows that the added light stabilizer could mitigate the transmission of asphalt components during the UV aging period. At the same time, the overall stability of the internal colloidal structure of asphalt is strengthened, and the aging resistance of asphalt is improved under the action of ultraviolet radiation.

Table 6: Aging index of characteristic functional groups of T622-modified asphalt

Aging time (h)	Index of characteristic functional groups		
	$I_{C=O}$	I_{Ar}	$I_{S=O}$
76.25	0.0209	0.0122	0.1481
152.5	0.0579	0.0277	0.1081
228	0.0599	0.0233	0.0445
305	0.0602	0.0298	0.1306

3.4 Physical and rheological properties of light stabilizer-modified asphalt

3.4.1 Physical property

3.4.1.1 Matrix asphalt

The physical properties of 70# matrix asphalt under different UV aging times are shown in Table 7. From Table 7, it could be seen that with the extension of UV aging time, the penetration of 70# matrix asphalt shows a significant downward trend, indicating that UV radiation would increase the hardness of asphalt. The softening point of asphalt is significantly increased with the extension of UV aging time, mainly due to the increase of heavy components in the asphalt, which leads to the increase of asphalt viscosity. The ductility of 70# matrix asphalt shows a significant decrease with the UV aging process, which is directly related

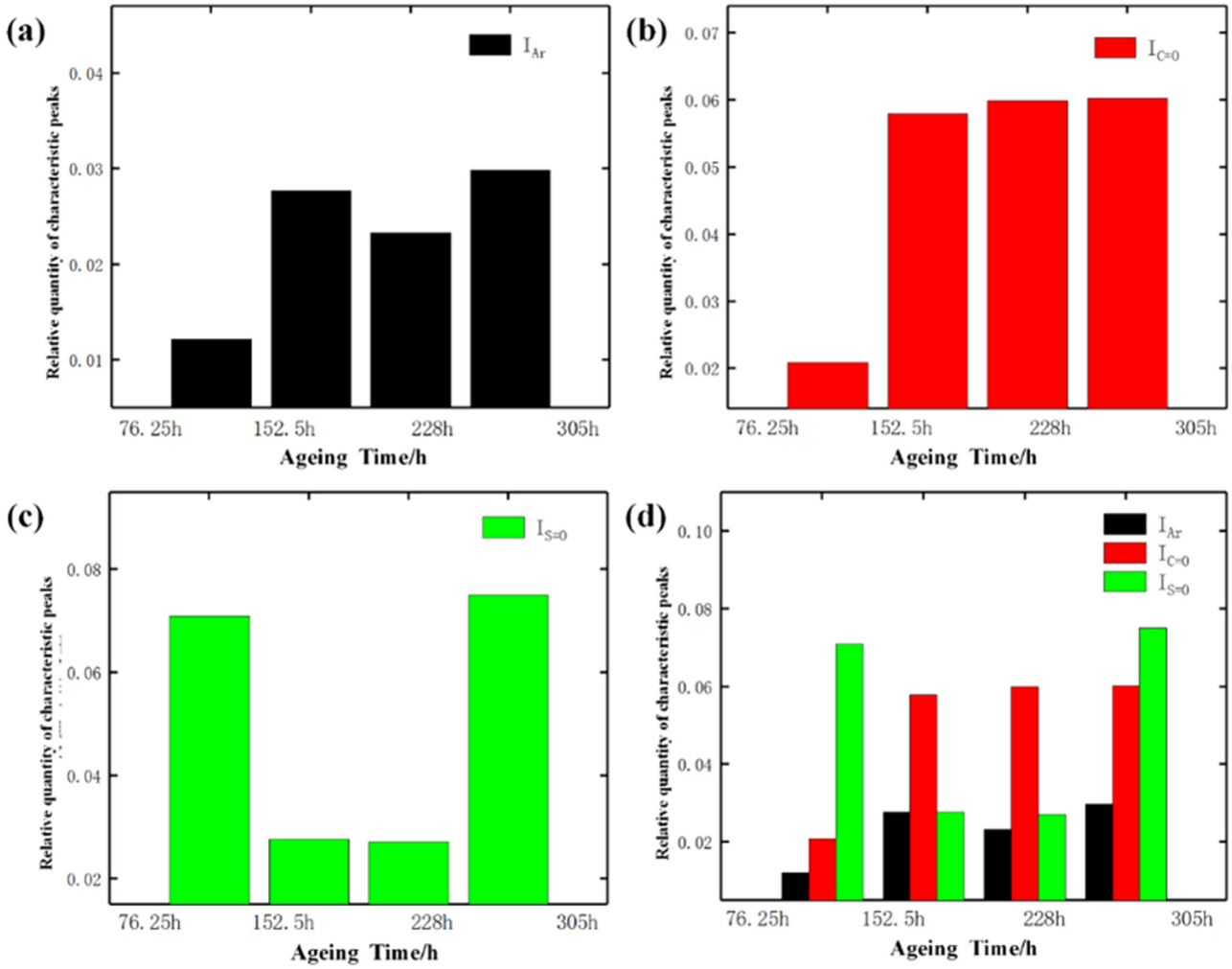

Figure 19: Aging index variation of characteristic functional groups of T622-modified asphalt. (a) I_{Ar}; (b) $I_{C=O}$; (c) $I_{S=O}$ and (d) Comparision.

to the degradation in deformability of the asphalt, and this is basically consistent with the change law of penetration. In summary, UV aging could cause the matrix asphalt to harden, manifested by the increase in the softening point and the significant decrease in penetration and ductility of the asphalt binder.

Table 7: Basic properties of 70# asphalt after UV aging

Aging time (h)	Penetration (0.1 mm)	Softening point (°C)	Ductility (cm)
76.25	47.4	48.7	17.1
152.5	45.1	51.4	14.5
228	42.0	55.8	11.2
305	41.3	59.4	9.5

3.4.1.2 T622 light stabilizer-modified asphalt

The physical performance test results of T622 light stabilizer-modified asphalt under different UV aging times are shown in Tables 8 and 10. According to the analysis in Table 8, there is a certain difference in the penetration difference of T622 light stabilizer-modified asphalt within the range of 0–305 h for UV aging. The penetration

Table 8: Penetration of ultraviolet aging T622 light stabilizer-modified asphalt

Aging time (h)	Penetration (25°C, 0.1 mm)			
	0.2%	0.4%	0.6%	0.8%
76.25	57.2	55.8	53.2	51.2
152.5	55.9	54.6	53	49.8
228	53.4	52.5	51.1	48.9
305	50.1	49.2	46.4	45.8

Table 9: Ductility of ultraviolet aging T622 light stabilizer-modified asphalt

Aging time (h)	Ductility (10°C, cm)			
	0.2%	0.4%	0.6%	0.8%
76.25	9.4	11.1	12.9	14.6
152.5	9.2	10.2	11.2	12.2
228	6.3	7.7	9	10.4
305	5.5	6.5	7.6	8.6

Table 10: Softening point of ultraviolet aging T622 light stabilizer-modified asphalt

Aging time (h)	Softening point (°C)			
	0.2%	0.4%	0.6%	0.8%
76.25	51.8	52.8	53.5	55.3
152.5	52.2	53.3	54.6	56.1
228	53.7	54.3	55.2	57.9
305	54.9	55.5	56.5	59.1

difference of modified asphalt before and after UV aging with the content of T622 light stabilizer 0.4% is the smallest, which indicates that the anti-aging performance of modified asphalt is optimal when the content of T622 light stabilizer is 0.4%. From Table 9, it could be seen that after 305 h of UV aging, the modified asphalt with the T622 light stabilizer content of 0.8% has the highest ductility difference, which is related to the improvement effect of light stabilizers on asphalt ductility. The difference in ductility between 0.2 and 0.4% T622 light stabilizer-modified asphalt before and after UV aging is the smallest, both around 4 cm. However, after UV aging, the ductility of modified asphalt of high content T662 is significantly higher than that of modified asphalt of low content. According to the analysis in Table 10, after 305 h of UV aging, the difference in softening points of T622 light stabilizer-modified asphalt with different modifier dosages is around 3°C, and there is no significant increase or change. This indicates that the T622 modifier could alleviate the impact of UV aging effectively on the high-temperature performance of asphalt, thereby achieving good UV aging resistance.

3.4.2 TS

Figure 20 shows the phase angle, complex modulus, and rutting factor of TS tests for 70# matrix asphalt and light stabilizer-modified asphalt, respectively. Through the analysis in Figure 20, it could be analyzed that the phase angle of different types of asphalt increases with temperature, which means that temperature change increases the viscosity of asphalt and reduces its elasticity. Meanwhile, with the extension of UV aging time, the phase angles of 70# matrix asphalt and light stabilizer-modified asphalt both significantly decrease, indicating that UV radiation could enhance the elastic response of asphalt, and the enhancement effect becomes more obvious with the extension of UV radiation time. It is worth noting that the phase angle of light stabilizer-modified asphalt decreases compared to the matrix asphalt with the decrease in UV irradiation time, indicating that T622 light stabilizer could enhance the anti-UV aging effect of asphalt binder. The complex modulus of different types of asphalt decreases gradually with temperature. As the UV aging time prolongs, the complex modulus of asphalt increases significantly, indicating that after the action of UV radiation, the asphalt binder exhibits varying degrees of hardening and its resistance to deformation is enhanced. Compared with the base asphalt, it could be found that the increase of the complex modulus of T622 light stabilizer-modified asphalt has significantly decreased, which proves that the anti-aging modifier has good anti-UV aging performance and could inhibit the significant changes of performance indices caused by UV radiation. Meanwhile, when the UV aging time is within the range of 76.25–152.5 h, the complex modulus difference of light stabilizer-modified asphalt is relatively small. With the extension of UV irradiation time, the difference of complex modulus of light stabilizer-modified asphalt becomes apparent gradually and the hardness increases significantly. This indicates that in the early stage of the UV radiation process, the influence of UV radiation on the deformation resistance of asphalt is not significant. As the UV radiation time continues to extend, its impact increases gradually, resulting in a significant increase in the hardness of the asphalt binder. The variation pattern of the rutting factor is basically consistent with the complex modulus, which gradually decreases with temperature, indicating that ultraviolet radiation could improve the deformation resistance of asphalt under high-temperature conditions. As the UV aging time prolongs, the improvement effect gradually strengthens. It is worth noting that compared to the base asphalt, the rutting factor difference of T622-modified asphalt is not significant between 76.25 and 152.5 h. As the UV aging time further extends, the rutting factor of T622 light stabilizer-modified asphalt decreases relatively, indicating that HALS could improve the UV aging resistance of asphalt binder.

3.4.3 BBR test

Table 11 shows BBR test results of T622 light stabilizer-modified asphalt. According to Table 11, at different UV

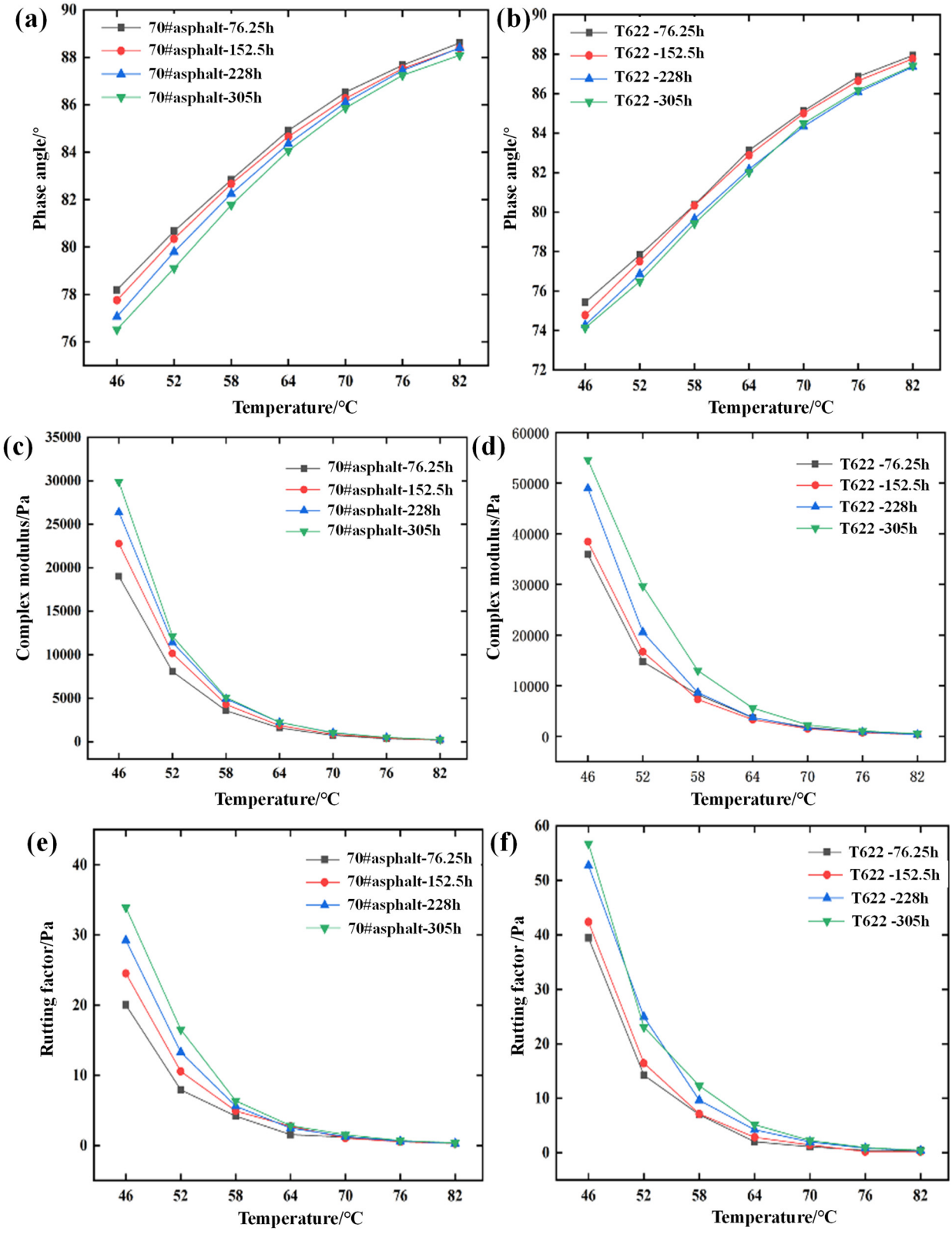

Figure 20: Phase angle, complex modulus, and rutting factor of base asphalt and modified asphalt at different UV aging times. (a) Phase angle-70# asphalt; (b) Phase angle-T622 modified asphalt; (c) Complex modulus-70# asphalt; (d) Complex modulus-T622 modified asphalt; (e) Rutting factor-70# asphalt and (f) Rutting factor-T622 modified asphalt.

Table 11: BBR test results

Asphalt	76.25 h		152.5 h		228 h		305 h	
	S **(MPa)**	***m***	***S*** **(MPa)**	***m***	***S*** **(MPa)**	***m***	***S*** **(MPa)**	***m***
70# asphalt	192	0.372	215	0.353	232	0.335	241	0.319
T662 asphalt	171	0.414	183	0.405	191	0.393	205	0.379

aging times, the creep modulus of T622 light stabilizer-modified asphalt is lower than that of 70# asphalt, and the creep rate is greater than that of 70# asphalt, which indicates that T622 light stabilizer could improve the low-temperature performance of asphalt directly. As the UV aging time prolongs, the creep modulus of asphalt shows an upward trend, while the creep rate decreases gradually. This indicates that within the range of 76.25–305 h, prolonging the aging time would degrade the low-temperature performance of asphalt. When the UV aging time is extended from 76.25 to 152.5, 228, and 305 h, the creep modulus *S* of 70# asphalt increases by 12, 21, and 25%, respectively, while the creep rate *m* decreases by 6, 11, and 15%. For T622 light stabilizer-modified asphalt, the creep modulus *S* increases by 7, 12, and 20% respectively, and the creep rate *m* decreases by 2, 5, and 8%. The rate of increase in creep modulus *S* and the rate of decrease in creep rate *m* are significantly lower than those of 70# asphalt. Therefore, it could be inferred that the T622 light stabilizer could reduce the impact of ultraviolet light on asphalt performance effectively and delay asphalt aging of asphalt.

4 Conclusions

1) The typical microstructure of T622-modified asphalt during the UV aging process is “fold structure”. The fold structure is essentially formed by the evolution of crack structures. The surface of T622-modified asphalt forms cracks with aging, and folds are formed due to the healing effect of asphalt.
2) At the four UV aging times, T622 light stabilizer-modified asphalt shows the maximum weight loss rate in sequence at 450–460°C. The temperature difference remains around 3°C and the temperature corresponding to the weight loss rate at the final aging time decreases to the lowest point of all aging times, indicating that T622 light stabilizer-modified asphalt would undergo early weight loss decomposition after long-term UV aging.
3) Although the T622 light stabilizer-modified asphalt would still produce corresponding functional groups under the influence of ultraviolet radiation, the growth rate and exponential growth amount of the relevant functional group are significantly lower than that of the base asphalt, which indicates that the light stabilizer could mitigate the transmission of asphalt components during the UV aging period.
4) As the UV aging process prolongs, T622-modified asphalt exhibits UV aging behavior from rheological properties, manifested by the decrease of phase angle, increase of rutting factor and complex modulus, and significant decrease of creep rate, which suggests that the elasticity and hardness of asphalt increase with UV aging time. The aging degree of light stabilizer-modified asphalt is significantly lower than that of 70# base asphalt, indicating that the addition of HALS could effectively improve the UV aging resistance of asphalt.
5) The mechanism of HALS on asphalt has been explored in this study preliminarily. In future studies, the correlation between the improving effect and mechanism would be expected to build, which could be provided reference for controlling the improving effect of HALS on the UV resistance of asphalt.

Acknowledgments: This paper describes research activities mainly requested and sponsored by Open Fund of National Engineering Research Center of Highway Maintenance Technology (Changsha University of Science& Technology) (kfj220104).

Funding information: This article describes research activities mainly sponsored by the Open Fund of National Engineering Research Center of Highway Maintenance Technology (Changsha University of Science & Technology) (kfj220104). That sponsorship and interest are gratefully acknowledged.

Author contributions: All authors contributed to the study conception and design. Material preparation, data collection, and analysis were performed by Wensheng Zhao, Guotao Fang, Xiao Qin, and Jie Mao. The first draft of the manuscript was written by Wensheng Zhao and all authors

commented on previous versions of the manuscript. All authors have accepted responsibility for the entire content of this manuscript and approved its submission.

Conflict of interest: The authors state no conflict of interest.

Data availability statement: All data generated or analyzed during this study are included in this published article.

References

[1] Li, Y., J. Feng, S. Wu, A. Chen, D. Kuang, Y. Gao, et al. Review of ultraviolet ageing mechanisms and anti-ageing methods for asphalt binders. *Journal of Road Engineering*, Vol. 2, 2022, id. 137–155.

[2] Liu, S., J. Jin, H. Yu, Y. Gao, Y. Du, X. Sun, et al. Performance enhancement of modified asphalt via coal gangue with microstructure control. *Construction and Building Materials*, Vol. 367, 2023, id. 130287.

[3] Sun, X., Z. Ou, Q. Xu, X. Qin, Y. Guo, J. Lin, et al. Feasibility analysis of resource application of waste incineration fly ash in asphalt pavement materials. *Environmental Science and Pollution Research*, Vol. 30, 2022, pp. 1–16.

[4] Sun, X., J. Yuan, Z. Liu, X. Qin, and Y. Yin. Evaluation and characterization on the segregation and dispersion of anti-UV aging modifying agent in asphalt binder. *Construction and Building Materials*, Vol. 289, 2021, id. 123204.

[5] Yin, F., E. Arámbula-Mercado, A. Epps Martin, D. Newcomb, and N. Tran. Long-term ageing of asphalt mixtures. *Road Materials and Pavement Design*, Vol. 18, 2017, pp. 2–27.

[6] Zhang, H., Z. Chen, G. Xu, and C. Shi. on of aging behaviors of asphalt binders through different rheological indices. *Fuel*, Vol. 221, 2018, pp. 78–88.

[7] Li, Y., S. Wu, Q. Liu, Y. Dai, C. Li, H. Li, et al. Aging degradation of asphalt binder by narrow-band UV radiations with a range of dominant wavelengths. *Construction and Building Materials*, Vol. 220, 2019, pp. 637–650.

[8] Yu, H., D. Yao, G. Qian, J. Cai, X. Gong, and L. Cheng. Effect of ultraviolet aging on dynamic mechanical properties of SBS modified asphalt mortar. *Construction and Building Materials*, Vol. 281, 2021, id. 122328.

[9] Sun, X., X. Qin, Z. Liu, Y. Yin, C. Zou, and S. Jiang. New preparation method of bitumen samples for UV aging behavior investigation. *Construction and Building Materials*, Vol. 233, 2020, id. 117278.

[10] Crucho, J., L. Picado-Santos, J. Neves, and S. Capitão. A review of nanomaterials' effect on mechanical performance and aging of asphalt mixtures. *Applied Sciences*, Vol. 9, 2019, id. 3657.

[11] Polo-Mendoza, R., G. Martinez-Arguelles, L. F. Walubita, F. Moreno-Navarro, F. Giustozzi, L. Fuentes et al. Ultraviolet ageing of bituminous materials: A comprehensive literature review from 2011 to 2022. *Construction and Building Materials*, Vol. 350, 2022, id. 128889.

[12] Xu, S., J. Yu, Y. Ke, L. Xue, and C. Hu. Preparation and anti-ultraviolet aging performance of organic layered double hydroxides/bitumen composites. *Journal of Wuhan University of Technology-Mater.* Sci. *Ed.*, Vol. 34, 2019, pp. 979–986.

[13] Liu, Z., X. Sun, X. Qin, and Y. Yin. Micro-analysis of the fusion process between light stabilizer and asphalt using different characterizing methods. *Construction and Building Materials*, Vol. 287, 2021, id. 123045.

[14] Ma, F., C. Zhu, Z. Fu, C. Li, Y. Hou, X. Jiang et al. Analysis of rheological behavior and anti-aging properties of SBS modified asphalt incorporating UV absorbent and naphthenic oil (NPO). *Construction and Building Materials*, Vol. 377, 2023, id. 130958.

[15] Liao, M., Z. Liu, Y. Gao, L. Liu, and S. Xiang. Study on UV aging resistance of nano-TiO2/montmorillonite/styrene-butadiene rubber composite modified asphalt based on rheological and microscopic properties. *Construction and Building Materials*, Vol. 301, 2021, id. 124108.

[16] Liu, L., Z. Liu, L. Hong, and Y. Huang. Effect of ultraviolet absorber (UV-531) on the properties of SBS-modified asphalt with different block ratios. *Construction and Building Materials*, Vol. 234, 2020, id. 117388.

[17] Liu, H., Z. Zhang, J. Xie, Z. Gui, N. Li, and Y. Xu. Analysis of OMMT strengthened UV aging-resistance of Sasobit/SBS modified asphalt: Its preparation, characterization and mechanism. *Journal of Cleaner Production*, Vol. 315, 2021, id. 128139.

[18] Guo, M., X. Liu, Y. Jiao, Y. Tan, and D. Luo. Rheological characterization of reversibility between aging and rejuvenation of common modified asphalt binders. *Construction and Building Materials*, Vol. 301, 2021, id. 124077.

[19] Qian, G., G. Yuan, D. Zhang, and Z. Li. Effect of Composite Light Stabilizer on the Anti-Ultraviolet Aging Property of Matrix Asphalt. *Journal of Materials in Civil Engineering*, Vol. 33, 2021, id. 04021176.

[20] Sun, X., Y. Zhang, Q. Peng, J. Yuan, Z. Cang, and J. Lv. Study on adaptability of rheological index of nano-PUA-modified asphalt based on geometric parameters of parallel plate. *Nanotechnology Reviews*, Vol. 10, 2021, pp. 1801–1811.

[21] Hodgson, J. L., and M. L. Coote. Clarifying the mechanism of the Denisov cycle: how do hindered amine light stabilizers protect polymer coatings from photo-oxidative degradation? *Macromolecules*, Vol. 43, 2010, pp. 4573–4583.

[22] Jiang, X., J. Gabrielson, H. Titi, B. Huang, Y. Bai, P. Polaczyk, et al. Field investigation and numerical analysis of an inverted pavement system in Tennessee, USA. *Transportation Geotechnics*, Vol. 35, 2022, id. 100759.

[23] Gryn'ova, G., K. U. Ingold, and M. L. Coote. New insights into the mechanism of amine/nitroxide cycling during the hindered amine light stabilizer inhibited oxidative degradation of polymers. *Journal of the American Chemical Society*, Vol. 134, 2012, pp. 12979–12988.

[24] Jiang, X., H. Titi, Y. Ma, P. Polaczyk, M. Zhang, J. Gabrielson, et al. Evaluating the performance of inverted pavement structure using the accelerated pavement test (APT). *Construction and Building Materials*, Vol. 346, 2022, id. 128489.

[25] Yu, H., Z. Zhu, Z. Leng, C. Wu, Z. Zhang, D. Wang, et al. Effect of mixing sequence on asphalt mixtures containing waste tire rubber and warm mix surfactants. *Journal of Cleaner Production*, Vol. 246, 2020, id. 119008.

[26] Jiang, X., J. Gabrielson, B. Huang, Y. Bai, P. Polaczyk, M. Zhang, et al. Evaluation of inverted pavement by structural condition indicators

from falling weight deflectometer. *Construction and Building Materials*, Vol. 319, 2022, id. 125991.

[27] Abouelsaad, A., and G. White. The combined effect of ultraviolet irradiation and temperature on hot mix asphalt mixture aging. *Sustainability*, Vol. 14, 2022, id. 5942.

[28] Gijsman, P., H. J. Smelt, and D. Schumann. Hindered amine light stabilizers: an alternative for radiation cross-linked UHMwPE implants. *Biomaterials*, Vol. 31, 2010, pp. 6685–6691.

[29] Feng, Z. G., H. J. Bian, X. J. Li, and J. Y. Yu. FTIR analysis of UV aging on bitumen and its fractions. *Materials and Structures*, Vol. 49, 2016, pp. 1381–1389.

[30] Xu, X., H. Guo, X. Wang, M. Zhang, Z. Wang, and B. Yang. Physical properties and anti-aging characteristics of asphalt modified with nano-zinc oxide powder. *Construction and Building Materials*, Vol. 224, 2019, pp. 732–742.

[31] Yu, H., X. Bai, G. Qian, H. Wei, X. Gong, J. Jin, et al. Impact of ultraviolet radiation on the aging properties of SBS-modified asphalt binders. *Polymers*, Vol. 11, 2019, id. 1111.

[32] Feczkó, T., M. Kovács, and Voncina, B. Improvement of fatigue resistance of spirooxazine in ethyl cellulose and poly (methyl methacrylate) nanoparticles using a hindered amine light stabilizer. *Journal of Photochemistry and Photobiology A: Chemistry*, Vol. 247, 2012, pp. 1–7.